

Os-Sr-Nd-Pb ISOTOPIC AND TRACE ELEMENT STUDY OF MAGMATIC  
PROCESSES WITHIN THE SIERRA DEL CHICHINAUTZIN VOLCANIC FIELD,  
TRANS-MEXICAN VOLCANIC BELT

A Thesis

Submitted to the

Faculty of Miami University

in partial fulfillment of

the requirements for the degree of

Master of Science

by

Brian Wright Cosky

Miami University

Oxford, OH

2010

Advisor \_\_\_\_\_  
Dr. Elisabeth Widom

Reader \_\_\_\_\_  
Dr. Mark P. Krekeler

## ABSTRACT

### Os-Sr-Nd-Pb ISOTOPIC AND TRACE ELEMENT STUDY OF MAGMATIC PROCESSES WITHIN THE SIERRA DEL CHICHINAUTZIN VOLCANIC FIELD, TRANS-MEXICAN VOLCANIC BELT

By Brian Wright Cosky

The petrogenetic processes that lead to compositional diversity in mafic volcanism of the Sierra Chichinautzin Volcanic Field (SCVF), central Mexico, are not well understood. This study involves an investigation of the trace element and Sr-Nd-Pb-Os isotope systematics, to constrain the relative roles of crustal assimilation versus subduction processes in generating enriched geochemical signatures in the mafic magmas of the SCVF. Both lower and upper crustal assimilation are ruled out, respectively, by the positive correlation of  $^{187}\text{Os}/^{188}\text{Os}$  and  $^{206}\text{Pb}/^{204}\text{Pb}$ , and the negative correlations between Pb/Ce and  $^{187}\text{Os}/^{188}\text{Os}$  and  $^{206}\text{Pb}/^{204}\text{Pb}$ . Rather, the data suggest that the compositional diversity of the SCVF magmas results from melting of a heterogeneous mantle wedge that has been metasomatized to variable degrees by hydrous fluids from the subducting altered oceanic crust and sediment, as well as a sediment melt component.

## Table of Contents

List of Tables.....	iii
List of Figures.....	iv
Acknowledgements.....	vi
Section 1. Introduction.....	1
Section 2. Geologic Setting and Background.....	2
Section 3. Sampling and Analytical Techniques.....	3
Section 4. Results.....	5
4.1 Major and Trace Elements.....	5
4.2 Isotopes.....	5
Section 5. Discussion.....	6
5.1 Mantle Source Heterogeneity Versus Crustal Assimilation.....	6
5.2 The Low-Nb End Member.....	8
5.3 The High-Nb End Member.....	9
5.3.1 Fluid Enrichment.....	10
5.3.2 Intra-Plate-Type Mantle.....	11
5.3.3 Slab Melting.....	11
5.3.4 Sediment Melting.....	11
5.4 Implications for the Behavior of Os During Subduction.....	12
Section 6. Conclusions.....	14
Tables.....	15
Figures.....	18
References.....	40

## **List of Tables**

Table 1. Major and Trace element data for samples from the SCVF and Jorullo

Table 2. Isotope data for samples from the SCVF and Jorullo

## List of Figures

Figure 1. TMVB map.....	18
Figure 2. SCVF map.....	19
Figure 3. Total alkali versus silica.....	20
Figure 4. Harker diagrams.....	21
Figure 5. Pearce diagram.....	22
Figure 6. Spider diagrams.....	23
Figure 7. $^{187}\text{Re}/^{188}\text{Os}$ versus Os concentration.....	24
Figure 8. $^{143}\text{Nd}/^{144}\text{Nd}$ versus $^{87}\text{Sr}/^{86}\text{Sr}$ .....	25
Figure 9. Osmium isotopic ratios versus Os concentration and MgO.....	26
Figure 10. $^{187}\text{Os}/^{188}\text{Os}$ versus $^{206}\text{Pb}/^{204}\text{Pb}$ .....	27
Figure 11. Trace Element Ratios versus MgO.....	28
Figure 12. $^{187}\text{Os}/^{188}\text{Os}$ versus Ba/Nb.....	29
Figure 13. Ba/La versus Nb/Yb.....	30
Figure 14. Pb Isotopic Ratios.....	31
Figure 15. Ba/Pb versus Pb Isotopic Ratios.....	32
Figure 16. Trace Element and Isotopic Ratios versus Pb/Ce.....	33
Figure 17. $^{143}\text{Nd}/^{144}\text{Nd}$ versus $^{87}\text{Sr}/^{86}\text{Sr}$ and $^{206}\text{Pb}/^{204}\text{Pb}$ versus $^{207}\text{Pb}/^{204}\text{Pb}$ .....	34
Figure 18. Zr/Hf versus Nb/Yb.....	35
Figure 19. Sr/Y versus Y.....	36
Figure 20. $^{206}\text{Pb}/^{204}\text{Pb}$ versus Zr/Hf and Nb/Ta versus Zr/Hf.....	37
Figure 21. Illustrated Model of the SCVF .....	38

Figure 22.  $^{187}\text{Os}/^{188}\text{Os}$  versus Ba/Zr .....39

## **Acknowledgements**

I would like to thank all the people who helped me to complete my thesis: to Dr. Elisabeth Widom, who has acted as both advisor and editor; to David Kuentz, for laboratory help and general guidance; to my fellow students under Dr. Widom, Zu Watanabe, Qing Meng, and Huimin Yu, for all their help; to Dr. John Morton, for his assistance with both the DCP and the ICP-MS; to Kim Wisman, for her support; and to my family and all friends whom I didn't mention by name. Financial support for this project came from both Dr. Widom's National Science Foundation grant (NSF EAR 1019798), from my Geological Society of America grant, and from the Miami University Geology Department.

## 1. Introduction

The study of subduction processes is important for understanding the formation of the continental crust, and how crustal recycling processes influence the evolution of the Earth's mantle. In subduction zones, oceanic sediments and seawater-altered oceanic lithosphere (or "slab") descend back into the mantle. Dehydration of the subducted materials releases fluids that infiltrate (or "metasomatize") the overlying peridotite of the mantle wedge, ultimately initiating melting and producing arc magmas (Tatsumi, 2005). Subduction-related basalts and andesites are typically "enriched" compared to normal mid-ocean-ridge basalts, with elevated concentrations of large-ion lithophile elements (LILE) and depletions in high field strength elements (HFSE). The geochemical signatures of subduction-related magmas likely reflect differences in the relative solubilities of these elements that lead to mobility of LILE and immobility of HFSE in slab-derived hydrous fluids (Tatsumi, 2005). Residual dehydrated slab materials are transported into the mantle, ultimately becoming incorporated as recycled crustal components in the shallow convecting mantle and possibly deep mantle plumes (Tatsumi, 2005).

In order to understand the fluxes of elements in subduction systems, and the effects of slab dehydration and relative element mobilities on the composition of resulting arc crust and the evolving mantle, it is important to be able to distinguish between geochemical signatures of magmas inherited from their mantle source regions versus those inherited during their ascent through the crust from source to surface. However, distinguishing between subduction-related geochemical signatures and those produced by shallow-level crustal assimilation is difficult, due to the similarity of the resulting geochemical signatures including relative LILE enrichments and HFSE depletions. The Re-Os isotope system has recently been shown to be a potentially important tracer that can distinguish between these respective petrogenetic processes, and is an ongoing area of active study in subduction systems (Alves et al., 2002; Lassiter and Luhr, 2001; Chesley et al., 2002).

Subduction zones are also the sites of much of the Earth's explosive volcanism, and thus important regions to understand from a volcanic hazards perspective. The Sierra Chichinautzin Volcanic Field in the Trans-Mexican Volcanic Belt is one of the world's most active monogenetic volcanic fields, with more than 200 Quaternary scoria cones. This region is also a heavily populated area close to Mexico City, where dense populations have grown on the slopes of the volcanoes (Siebe et al., 2006). Deciphering the petrogenetic processes in areas such as this is important for better evaluating the potential hazards associated with subduction-related monogenetic volcanism.

This study focuses on the use of the Re-Os isotope system, in combination with Sr, Nd and Pb isotope and trace element analysis, to evaluate the petrogenetic processes operating in the Sierra Chichinautzin Volcanic Field. Enriched geochemical signatures in volcanic rocks of the Trans-Mexican Volcanic Belt, including those of the Sierra Chichinautzin Volcanic Field, have been variously attributed to either a subduction-related history or lower crustal assimilation (Alves et al., 2002; Lassiter and Luhr, 2001; Chesley et al., 2002). This study aims to reevaluate the importance of subduction-fluid metasomatism of the mantle wedge versus lower or upper crustal assimilation in the petrogenesis of the Sierra Chichinautzin Volcanic Field.

## 2. Geologic Setting and Background

The Trans-Mexican Volcanic Belt (TMVB) is an ~1,000 km long volcanic province located in the center of Mexico, south of the Sierra Madre Occidental (Fig. 1). The TMVB cuts across Mexico transversely from the Gulf of California to the Gulf of Mexico, in an approximately east-west orientation. The volcanoes of the TMVB, as well as associated dikes, occur along lineaments that are controlled by normal and transtensional faults that may serve as magmatic conduits (Ferrari et al., 2000).

The TMVB is thought to be related to the subduction of the Rivera and Cocos plates beneath the North American plate, which has resulted in volcanism in the area since the Miocene (Ferrari et al., 2000; Ortega-Gutierrez et al., 2008). An unusual feature of the TMVB subduction system is the oblique (~16°) angle of the volcanic belt relative to the orientation of the Middle-American Trench (Fig. 1), attributed to a shallowing of the dip angle of the subducting plates from west to east due to variable slab age and convergence rates (Pardo and Suarez, 1995; Blatter et al., 2007). The TMVB is divided into three sections based on changes in composition, the nature of the volcanism, and structural differences (Ortega-Gutierrez et al., 2008; Wallace and Carmichael, 1999). The western section extends roughly from Parícutin to the Pacific Ocean; the central section extends roughly from Parícutin in the west to Popocatepetl in the east; and the eastern section extends roughly from Popocatepetl to the Gulf of Mexico (Ortega-Gutierrez et al., 2008).

The Sierra Chichinautzin Volcanic Field (SCVF) is located primarily in the Central section of the TMVB, just south of Mexico City (Fig. 2). It is an E-W oriented volcanic highland extending from Popocatepetl in the east to Nevado de Toluca in the west. An east-west fracture pattern (Fries, 1962; Mooser, 1962) and the east-west alignment of the volcanic centers are indicative of a north-south extensional stress (Siebe et al., 2004). The structure of the SCVF has been interpreted as an east-west trending horst defined by a northern E-W trending fault that dips north, and a southern E-W trending fault that dips south (Siebe et al., 2004). The basement rocks include Cretaceous marine clastic limestones and dolomites (>3 km thick) and Tertiary lahars (> 1 km thick) containing dacitic and andesitic clasts; outcrops of the basement are found in the south of the SCVF in Cuernavaca and Cuautla valleys (Siebe et al., 2004).

The SCVF is interpreted to be the volcanic front of the TMVB in this area (Siebe et al., 2004). The SCVF has one of the highest concentrations of monogenetic volcanoes in the TMVB, including 220 Quaternary scoria cones, flows and shields over a 2500 km<sup>2</sup> area (Bloomfield, 1975; Martin, 1982). The volcanic rocks of the SCVF comprise basalts, basaltic andesites, andesites, and dacites, most of which are calc-alkaline or sub-alkaline (Gunn and Mooser, 1971; Swinamer, 1989; Siebe et al., 2004). Trace element signatures suggest that the SCVF magmas fall into two broad categories: one group is characterized by LILE enrichment and HFSE depletion and is thus typical of subduction-related magmatism; the other is characterized by LILE enrichment but lacks HFSE depletion, and thus is less easily related to subduction processes.

The compositional variability of the volcanic rocks, as well as the associated tectonic complexities, have led to some controversy regarding the role of subduction in the development of the TMVB. From a tectonic perspective, if the SCVF is the front of the TMVB, then the subducting slab (Cocos plate) should be at a depth of ~110-120km

beneath this region, as is typical of most arc volcanic fronts (Marquez et al., 1999). However, the depth-to-slab beneath the SCVF is inferred to be only ~80-100km. From a geochemical perspective, rocks of the SCVF produce a dominantly calc-alkaline trend as expected in subduction zones (Marquez et al., 1999). However, some of the most mafic rocks have chemical affinities with ocean island basalts (OIB) including the lack of negative Nb anomalies, and thus have an “intra-plate” character. Although andesites and dacites do show the negative Nb and Ti anomalies typical of subduction zones, this could be due to shallow level crustal assimilation. Sr and Nd isotopic ratios of most SCVF rocks fall within the mantle array defined by mid-ocean-ridge and ocean island basalts, and thus do not clearly demonstrate subduction signatures (Siebe et al., 2004). Although it has been suggested that the intra-plate geochemical character of some of the TMVB volcanic rocks could be attributed to a mantle plume (Marquez et al., 1999), this model is problematic in that OIB-type lavas account for only a small percent of TMVB lavas (~5%, Ferrari et al., 2001). Furthermore, a plume should result in a temporal and spatial progression of uplift, extension and volcanism that is not supported by the field observations in the TMVB (Ferrari et al., 2001).

### **3. Sampling and Analytical Techniques**

Nine lava samples were chosen for this study, including eight from the SCVF and one from Jorullo volcano, further to the west in the TMVB. Samples were selected based on their high Ni and MgO contents (Table 1), representing some of the least evolved lavas found within and near the SCVF, including seven basaltic andesites and two basalts. Samples from the SCVF are from the area south of Mexico City, including Xitle (1670 BP), Popocatepetl, Chichinautzin (1835 BP), Cilcuayo (near Tlaloc, 6200 BP), and Pelegatos (near Tlaloc). The lava samples are porphyritic and contain olivine and clinopyroxene phenocrysts (Siebe et al., 2004).

Three samples of potential upper crustal assimilants were also analyzed, including a quartz-rich cumulate xenolith from the Chichinautzin volcanic center ~20 km south of Mexico City, and an andesite clast from a Tertiary lahar flow and Cretaceous carbonate basement (micritic limestone), both collected at Tepoztlan ~30 km south of Mexico City.

All samples were prepared by sawing into ~1/4” thick slices. Metal from the saw blade was removed from the surfaces of the slices by grinding with silicon carbide sandpaper. Samples were then rinsed with de-ionized water and cleaned in an ultrasonic bath several times. After drying overnight in an oven, the rock slices were wrapped in Ziploc bags and several layers of paper, and broken with a hammer to produce pieces ~1/4” in maximum dimension. These pieces were then processed in an alumina jaw crusher prior to powdering in a high purity alumina shatterbox. These procedures ensured that the samples were free from any metal contamination that could potentially contaminate the samples with Re and/or Os.

Major elements were analyzed on a Beckman SpectraspanV Direct-Current Plasma Atomic Emission Spectrometer (DCP-AES) at Miami University following the sample preparation and measurement methods of Katoh et al. (1999). Sample powders (10 mg) were dissolved using a lithium metaborate flux fusion procedure followed by dissolution in weak (~1%) nitric acid. Major element analyses were calibrated based on regressions of international rock standards, including RGM-1, BCR-2, AGV-1, GSP-2,

BHVO-2, W-2, BE-N, NIM-G, AN-G, and SY-2. Trace element analyses were done using the standard additions technique (Kato et al., 1999). Corrections for instrumental drift during the analysis periods were performed using Ge as an internal standard.

Trace elements were analyzed using a Varian Inductively Coupled Plasma Mass Spectrometer (ICP-MS). Sample preparation for ICP-MS analysis involved dissolution of ~300 mg of sample powder in a similar amount of NaBO<sub>3</sub> flux. Samples were fused in graphite crucibles at 950°C for 20 minutes. The resulting glass beads were then crushed by a small anvil, and further crushed beneath “the rocker,” a curved metal bar that rocks side-to-side to more fully crush the beads. Once the fused beads were crushed sufficiently, 100 mg of each sample was weighed into a Savillex beaker; 6mL of HNO<sub>3</sub>, 3mL of HF, and 0.5mL of HClO<sub>4</sub> were then added to the beakers, and the beakers placed on a hotplate on high heat until dissolved. Following dissolution, the samples were dried down and then redissolved in 3 ml of 1N HNO<sub>3</sub>, and transferred to clean polyethylene bottles in preparation for analysis by ICP-MS. Analyses were performed using calibrations based on international rock standards, and using <sup>115</sup>In and <sup>185</sup>Re as internal standards to correct for within-run instrumental drift.

For Pb, Nd, and Sr isotopic analyses, 0.1g of sample powder was dissolved by acid digestion using a 2:1 ratio of HF to HNO<sub>3</sub>, and placed overnight on a hot plate at ~80°C. Samples were dried down and redissolved multiple times in HNO<sub>3</sub>, followed by final dissolution in 0.5N HBr in preparation for Pb separation by anion exchange column chemistry using HBr and HNO<sub>3</sub>. Sr separations were done using EiChrom Sr-spec resin in weak HCl. The residue from the Sr columns was processed through cation columns in HCl to separate the rare earth elements (REE), which were then passed through EiChrom Ln-spec resin in weak HCl to separate Nd from Sm. Details of the separation procedures for Pb, Sr, and the REEs can be found in Walker et al., (1989) and Snyder (2005). Sm-Nd separations were done using methods similar to those of Pin and Zalduegui (1997) and Snyder (2005).

For Re-Os chemistry, samples were digested in Carius tubes using the method developed by Shirey and Walker (1989), in which samples are dissolved in reverse aqua regia at 240 degrees C for ~48 hours. Re and Os were separated by a solvent extraction technique in which Os is extracted from the reverse aqua regia into CCl<sub>4</sub>, and then back extracted into HBr (Cohen and Waters, 1996). After drying down the HBr, the Os was further purified by a microdistillation technique in which 30 µl of chromium tetroxide was added as an oxidant, and the volatile Os trapped in 20 µl of HBr (Roy-Barman, 1993; Roy-Barman and Allegre, 1995).

Sr, Nd, Pb and Os isotopic compositions, and Re and Os concentrations were obtained on a Finnigan Triton thermal ionization mass spectrometer at Miami University. Sr samples were loaded onto single Ta filaments with a Ta<sub>2</sub>O<sub>5</sub> activator, and Pb was loaded onto single Re filaments with silica gel and phosphoric acid, which helps inhibit rapid volatilization. Nd was loaded onto double Re filaments as a nitrate, with phosphoric acid. Re and Os were loaded onto single platinum filaments with BaNO<sub>3</sub> and BaOH activators, respectively. Sr, Nd and Pb were run as positive ions of the respective metals. Internal mass fractionation corrections for Sr and Nd were based on the exponential law, with <sup>86</sup>Sr/<sup>88</sup>Sr=0.1194 and <sup>144</sup>Nd/<sup>146</sup>Nd=0.7219. External mass fractionation corrections for Pb isotope analyses were based on long-term results on the NBS981 Pb standard relative to the accepted values of Todt et al. (1996), from which fractionation corrections

of 0.11% per amu have been established. Os and Re isotopes were measured as the negative molecular ions of  $\text{OsO}_3^-$  and  $\text{ReO}_4^-$ , respectively. Osmium isotope ratios were corrected for oxygen isotopes based on the oxygen isotopic composition of Nier (1950). Mass fractionation correction for Os was based on  $^{192}\text{Os}/^{188}\text{Os}=3.0826$ . External reproducibilities of the isotopic ratios based on 2 standard deviations (2 S.D.) of the mean of numerous standard measurements during the period of the analyses for this study are as follows:  $^{87}\text{Sr}/^{86}\text{Sr} = \pm 0.000015$ ;  $^{143}\text{Nd}/^{144}\text{Nd} = \pm 0.000007$ ;  $^{206}\text{Pb}/^{204}\text{Pb} = \pm 0.015$ ;  $^{207}\text{Pb}/^{204}\text{Pb} = \pm 0.020$ ;  $^{208}\text{Pb}/^{204}\text{Pb} = \pm 0.063$ ;  $^{187}\text{Os}/^{188}\text{Os} = \pm 0.0002$ .

## 4. Results

### 4.1 Major and Trace Elements

The SCVF and Jorullo samples were selected to represent a range of less evolved lavas from the respective volcanic fields.  $\text{SiO}_2$  concentrations range from ~51-57 wt. %, and MgO from 7.8 to 10.1 wt.% (Table 1). On an alkalis versus  $\text{SiO}_2$  diagram (Fig. 3), all samples are sub-alkaline and range from basalt to basaltic andesite. Correlations of major element oxides versus MgO (Fig. 4) are quite scattered, consistent with the lavas coming from different monogenetic vents that have evolved in separate magmatic systems. Nevertheless, in general, with decreasing MgO the samples exhibit an overall decrease in CaO, and increase in  $\text{SiO}_2$ ,  $\text{Al}_2\text{O}_3$ ,  $\text{K}_2\text{O}$ ,  $\text{Na}_2\text{O}$  and  $\text{P}_2\text{O}_5$ , broadly consistent with magma evolution governed by fractionation of olivine and clinopyroxene with only limited plagioclase fractionation.

Trace elements signatures also suggest that the lava samples are primarily calc-alkaline in nature, although a few exhibit transitional intra-plate characteristics on a Zr-Ti/100-Y\*3 ternary Pearce element discrimination diagram (Fig. 5). On N-MORB normalized spider diagrams (Fig. 6), all samples are strongly light rare earth element (LREE) enriched, and none exhibit negative Eu anomalies, further confirming that plagioclase has not been an important fractionating mineral phase during the evolution of these magmas. In addition, all of the samples exhibit positive Cs, Ba, K, Pb and Sr anomalies, characteristic of typical subduction-related magmas. However, the samples can be divided into two groups based on the behavior of Nb, with some samples exhibiting strong negative Nb anomalies characteristic of subduction-related magmas, and others lacking strong negative Nb anomalies.

Re and Os concentrations in the lavas range from 0.029-0.093 ppb and 0.012-0.150 ppb, respectively (Table 2). The samples fall at the high Os, low Re/Os end of the range for typical arc lavas, and extend the previous range for TMVB to higher Os concentrations (Fig. 7). Os exhibits a scattered but negative correlation with MgO, and Re and Re/Os are negatively correlated with Os, consistent with the compatible behavior of Os and incompatible behavior of Re, respectively.

### 4.2 Isotopes

Sr, Nd, Pb and Os isotopic compositions have been obtained for whole rock samples from the SCVF (Table 2). The lava samples exhibit significant isotopic heterogeneity, with  $^{87}\text{Sr}/^{86}\text{Sr}$  varying from 0.70360 to 0.70419,  $^{143}\text{Nd}/^{144}\text{Nd}$  from 0.51281

to 0.51293, and  $^{206}\text{Pb}/^{204}\text{Pb}$  from 18.63 to 18.76. Sr and Nd isotopic compositions are, respectively, more and less radiogenic than normal MORB (N-MORB) including that from the East Pacific Rise (EPR), but are typical of other arc magmas and within the range found previously for other TMVB lavas (Fig. 8). The Tertiary andesite xenolith falls within the range of the SCVF lavas for Sr and Nd isotopes, and within analytical error for Pb isotopes, whereas the quartz-rich cumulate xenolith is substantially more radiogenic in Sr ( $^{87}\text{Sr}/^{86}\text{Sr} = 0.71213$ ) and less radiogenic in Nd ( $^{143}\text{Nd}/^{144}\text{Nd} = 0.51242$ ). The carbonate basement sample has a moderately radiogenic Sr isotopic signature consistent with Cretaceous seawater ( $^{87}\text{Sr}/^{86}\text{Sr} = 0.7073$ ; Mearon et al. 2003), and a very radiogenic Pb isotope signature with  $^{206}\text{Pb}/^{204}\text{Pb}$  of 22.29.

Os isotope ratios in the lavas also exhibit a large range, with  $^{187}\text{Os}/^{188}\text{Os}$  varying from 0.1329 to 0.2608, all significantly more radiogenic than depleted MORB mantle ( $^{187}\text{Os}/^{188}\text{Os} = 0.122\text{-}0.127$ ; Snow and Reisberg, 1995). Os isotope ratios are negatively correlated with MgO and Os concentration (Fig. 9), and positively correlated with  $^{206}\text{Pb}/^{204}\text{Pb}$  (Fig. 10). The Tertiary andesite xenolith has a  $^{187}\text{Os}/^{188}\text{Os}$  ratio of 0.242, similar to the most radiogenic SCVF lavas, and consistent with its relatively low Os concentration (0.011 ppb). The quartz-rich cumulate xenolith and carbonate basement sample also have low Os abundances (0.002 and 0.019 ppb) and are substantially more radiogenic than the lavas, with  $^{187}\text{Os}/^{188}\text{Os}$  of 0.4735 and 1.1798, respectively.

## 5. Discussion

All of the lava samples have enriched isotopic signatures compared to N-MORB, and all are strongly LREE-enriched and exhibit positive Cs, Ba, K, Pb and Sr anomalies. However, the variable isotope signatures and the respective presence or absence of strong negative Nb anomalies indicate that multiple sources contribute to the petrogenesis of these lavas. The trace element and isotopic variations together suggest that the samples comprise two endmember compositional groups: a less enriched group with lower  $^{87}\text{Sr}/^{86}\text{Sr}$  and  $^{206}\text{Pb}/^{204}\text{Pb}$  and strong negative Nb anomalies (the “low-Nb” group) exemplified by samples JOR 0611, PG05-16, and PG05-18, and a more enriched group with higher  $^{87}\text{Sr}/^{86}\text{Sr}$  and  $^{206}\text{Pb}/^{204}\text{Pb}$  and lacking strong negative Nb anomalies (the “high-Nb” group), as represented by samples B3-06, 00-00, PO 0569, and PG05-19. The petrogenesis of the two end member compositional groups, including the relative roles of heterogeneous mantle sources and crustal assimilation, are further explored below.

### 5.1. Mantle source heterogeneity versus crustal assimilation

The lava samples selected for this study represent relatively unevolved, high MgO basalts and basaltic andesites, selected in order to minimize potential effects of crustal assimilation that commonly affect more evolved magmas. However, even for mafic samples, it is important to investigate the potential role of crustal assimilation, which could imprint enriched trace element and isotopic signatures on the magmas. Potential effects of crustal assimilation can be assessed by investigating the relationship of isotopic signatures and highly incompatible trace element ratios with indices of fractionation, as geochemical signatures resulting from crustal assimilation will generally be more

pronounced in samples that have undergone a greater extent of fractionation (i.e. greater extents of combined assimilation-fractional crystallization, or AFC; DePaolo, 1981).

Os isotopes are arguably the most sensitive isotopic tracer of crustal assimilation, due to the order-of-magnitude difference between the Os isotope signatures of crustal versus mantle-derived rocks (e.g. Widom and Shirey, 1996). The negative correlations of  $^{187}\text{Os}/^{188}\text{Os}$  with Os concentration and MgO (Fig. 9) are consistent with the possibility that the Chichinautzin samples have been affected by crustal AFC processes. Previous studies of relatively mafic lavas from the TMVB, including a few samples from the SCVF, have argued that such correlations can be attributed to assimilation of lower continental crust (Lassiter and Luhr, 2001; Chesley et al., 2002). However, the positive correlation of  $^{187}\text{Os}/^{188}\text{Os}$  with  $^{206}\text{Pb}/^{204}\text{Pb}$  (Fig. 10) is opposite that expected for assimilation of lower crust, and potentially consistent only with assimilation of upper crust. Furthermore, although the lava samples in this study exhibit a weak negative trend ( $r^2=0.41$ ) of  $^{187}\text{Os}/^{188}\text{Os}$  with MgO (Fig. 9), this is primarily controlled by a single sample (PO 0569) with low MgO and radiogenic Os. If this sample is excluded, there is no apparent correlation ( $r^2=0.13$ ) of Os isotopes with MgO. Hence, the potential role of crustal assimilation needs to be further evaluated.

The pronounced positive Pb anomaly (Fig. 6) and associated low Ce/Pb ratios observed in all of the lava samples are characteristics of continental crust and marine sediment (e.g. Rudnick and Gao, 2003; Plank and Langmuir, 1998) and could potentially be imparted to the magma either by crustal assimilation or subduction-related metasomatism of the mantle wedge. Because Ce/Pb ratios are not affected by variable degrees of partial melting of the mantle or fractional crystallization of basaltic magmas, this ratio is a robust tracer of the sources that contribute to the magmas. The scattered but negative correlation between Ce/Pb and MgO (Fig. 11a) argues against the importance of crustal AFC processes, whether involving average upper or lower crust or any of the crustal lithologies analyzed in this study, in controlling the composition of these magmas. Similar conclusions can be made with regard to the positive Ba and variable negative Nb anomalies in the lava samples. Although the lava samples have high Ba/Nb, Ba/Zr and Ba/La relative to MORB (Fig. 11b,c,d), all of which are compositional characteristics of continental crust, the lack of correlation with MgO is inconsistent with crustal AFC processes controlling the magma compositions. In particular, the scattered but positive trend of Ba/Zr vs. MgO (Fig. 11c) is precisely opposite that expected for crustal AFC.

Evidence from trace element ratios combined with Os isotope signatures allows further evaluation of the potential role for crustal assimilation. On a plot of  $^{187}\text{Os}/^{188}\text{Os}$  vs. Ba/Nb (Fig. 12), the SCVF lavas exhibit a strongly hyperbolic trend that is consistent with a two component mixing process between one endmember with relatively high Ba/Nb ( $>100$ ) and low  $^{187}\text{Os}/^{188}\text{Os}$  ( $<0.133$ ) and a second endmember with relatively low Ba/Nb ( $\approx 20$ ) and high  $^{187}\text{Os}/^{188}\text{Os}$  ( $>0.261$ ). In contrast to both of these mixing endmembers, upper and lower crust are both characterized by intermediate Ba/Nb combined with radiogenic Os, hence continental crust cannot explain either of the endmembers in the two-component hyperbolic mixing trend exhibited by the SCVF lavas (Fig. 12). Given the apparent inconsistencies with the involvement of crustal AFC processes in the petrogenesis of the SCVF lavas, alternative explanations for the chemical and isotopic variations in the lavas are considered below.

## 5.2. The Low-Nb End Member

The low-Nb group samples are characterized by strong positive Cs, Ba, K, Pb and Sr anomalies and negative Nb, Ta, and Ti anomalies relative to N-MORB (Fig. 6), which are typical subduction signatures that can be attributed broadly to the mobility of LILE and immobility of HFSE during dewatering of subducted materials (Gill, 1981; Pearce et al., 2005), possibly in part controlled by the strong retention of HFSE in residual rutile or other phases during dewatering (Brenan et al., 1994; Brenan et al., 1995). Potential sources of fluids to the mantle wedge include water released from the hydrated, altered oceanic lithosphere and subducted sediments. The nature and degree of fluid addition to the mantle wedge can best be elucidated by the relationships between element pairs that have similar partition coefficients during mantle melting but variable fluid mobility, whereas compositional characteristics of the pre-subduction mantle wedge are best revealed by ratios of elements that are fluid immobile and have different partition coefficients during mantle melting (Pearce and Peate, 1998). Diagrams such as Ba/La vs. Nb/Yb are therefore particularly diagnostic in that Nb/Yb serves as an indicator of the degree of melt depletion of the pre-subduction mantle wedge ( $D_{\text{Nb}} < D_{\text{Yb}}$ ), and Ba/La serves as an indicator of fluid addition to the wedge given the much greater fluid mobility of Ba relative to La.

The SCVF lavas produce a coherent negative trend of Ba/La vs. Nb/Yb, with all samples exhibiting higher Ba/La and Nb/Yb than N-MORB (Fig. 13), and the low-Nb group samples having substantially higher Ba/La and lower Nb/Yb than the more high-Nb group samples. These systematics are consistent with variable degrees of fluid addition to a variably depleted mantle wedge, in which the low-Nb group samples are produced by melting of a more strongly melt depleted mantle wedge (lower Nb/Yb) that has experienced greater fluid addition (higher Ba/La). Both sediments and altered oceanic crust are potential sources of high Ba/La fluids, as both have elevated Ba/La ratios relative to N-MORB, and fluids generated during dewatering will further concentrate Ba relative to La due to the greater fluid mobility of the former (Kogiso et al., 1997).

The potential involvement of altered oceanic crust- and sediment-derived fluids can be further evaluated by investigating the behavior of Pb, one of the very most fluid-mobile elements (Kogiso et al., 1997). Pacific MORB, including East Pacific Rise (EPR) MORB from the vicinity of the TMVB between 15-19 degrees North, exhibits a large range in Pb isotopic values, which makes it difficult to determine the Pb isotopic composition of pre-subduction mantle wedge in this region. Nevertheless, the SCVF lavas display a large range in Pb isotopes and produce trends in Pb-Pb isotope space that are distinct from that of Pacific MORB (Fig. 14). Of particular note is the observation that the Pb isotope ratios of the SCVF lavas span a mixing space that is essentially bounded at both ends by the pelagic and the hemipelagic sediment groups of the DSDP 487 core sampled at the Cocos trench due south of Chichinautzin. This suggests that the Pb isotopic compositions of the lavas could be largely controlled by a sediment-derived Pb flux (LaGatta, 2003). However, although such a model is consistent with both the  $^{207}\text{Pb}/^{204}\text{Pb}$ - $^{206}\text{Pb}/^{204}\text{Pb}$  (Fig. 14a) and  $^{208}\text{Pb}/^{204}\text{Pb}$ - $^{206}\text{Pb}/^{204}\text{Pb}$  (Fig. 14b) trends, variations in  $^{207}\text{Pb}/^{204}\text{Pb}$ - $^{208}\text{Pb}/^{204}\text{Pb}$  (Fig. 14c) suggest that the low-Nb mixing endmember trends toward a composition with lower  $^{207}\text{Pb}/^{204}\text{Pb}$  for a given  $^{208}\text{Pb}/^{204}\text{Pb}$  than any pelagic sediment. This could reflect the contribution of fluid derived from the subducted altered

oceanic crust, since this would have the same Pb isotopic compositions as local MORB (i.e. Pb is not significantly affected by seafloor alteration; Kelley et al., 2003; DuFrane et al., 2009); however, the similarity of the overall range in Pb isotopes of the SCVF lavas and subducting sediments warrants further evaluation of the involvement of sediment-derived fluid.

Variations in Ba/Pb ratios of the SCVF lavas provide additional insight. The SCVF lavas exhibit a small but significant range in Ba/Pb, with the low-Nb group samples having lower Ba/Pb ratios (Fig. 15). Furthermore, all of the SCVF lavas have higher Ba/Pb ratios than both N-MORB and altered oceanic crust. Given the relative mobilities of Pb and Ba, a hydrous fluid should have a lower Ba/Pb ratio than the source from which it is derived. This is inconsistent with the source of the SCVF lavas being derived from a depleted mantle wedge metasomatized by fluids solely from altered oceanic crust. Rather, the relatively high Ba/Pb ratios of the SCVF lavas appear to require addition of fluid derived from subducting sediment. Pelagic sediment from the DSDP 487 core has high Ba and Pb concentrations and Ba/Pb ratios higher than those of the SCVF lavas, and is thus a likely source of both Ba and Pb to the mantle source of the low-Nb group samples.

The relative contributions of altered oceanic crust-derived and sediment-derived fluids to the mantle source of the low-Nb group lavas can be broadly constrained by considering the Ba and Pb concentrations in the subducting altered oceanic crust and pelagic sediment, and the fluid mobilities of the respective elements. Using the Ba and Pb concentrations of the DSDP 487 average pelagic sediment (LaGatta 2003) and altered oceanic crust (Gomez-Tuena et al., 2007), water contents of composite altered oceanic crust and subducting sediment (Kelley et al., 2003), and the solid-fluid partition coefficients for Ba and Pb (Kogiso et al., 1997), Ba and Pb concentrations and Ba/Pb ratios can be calculated for likely fluids derived from subduction dewatering of DSDP 487 altered oceanic crust and pelagic sediment. The resulting fluid compositions, based on the equation of Tatsumi and Kogiso (1997), are as follows: altered oceanic crust-derived fluid: Pb = 3 ppm, Ba = 69 ppm, Ba/Pb = 21; pelagic sediment-derived fluid: Pb = 274 ppm, Ba = 16,841 ppm, Ba/Pb = 62. Two-component mixing calculations given these fluid compositions and the Ba/Pb ratio (~55) observed in the low-Nb group SCVF lavas suggest that approximately 94% of the fluid was derived from the altered oceanic crust, and 6% from the pelagic sediment. This result is consistent with that of many other arcs globally, for which altered oceanic crust likely contributes 70-96% of the subduction fluid (Morris et al., 1990). However, the Pb and Ba budgets are dominated by the sediment-derived fluid component even with only 6% of the fluid being sediment-derived, due to the very high Pb and Ba concentrations of the sediment-derived fluid. For a 6% fluid contribution from the sediment, 84% of the Pb and 94% of the Ba in the subduction fluid is sediment-derived. This is consistent with the Pb isotope ratios of the low-Nb group samples, which are very close to those of the pelagic sediment.

### *5.3. The High-Nb End Member*

The high-Nb group samples exhibit similar major element systematics to those in the low-Nb group, spanning a similar range in MgO from ~8-10%, although generally exhibiting slightly lower SiO<sub>2</sub> and higher TiO<sub>2</sub> and P<sub>2</sub>O<sub>5</sub> for a given MgO (Table 1 and

Fig. 4). The higher  $\text{TiO}_2$  results in the high-Nb group samples falling in a transitional region between calc-alkaline and intra-plate compositions on the ternary Pearce element discrimination diagram (Fig. 5).

The high-Nb group samples share some of the trace element characteristics of the low-Nb group, including enrichments relative to N-MORB in the fluid mobile elements Cs, Ba, K, Pb and Sr. However, the high-Nb group samples differ from the low-Nb group in their abundances of nominally fluid immobile elements including HFSE and REE. Compared to the low-Nb group, the high-Nb group samples exhibit slightly greater enrichments relative to N-MORB of Th, U, P, Zr and light- to middle-REE, and less depletion in HREE. The most significant distinction is the lack of significant negative Nb and Ti anomalies that are characteristic of typical subduction-related magmas and the low-Nb group samples (Fig. 6).

The high-Nb group samples are also distinct from the low-Nb group samples in that they are less radiogenic in Sr and generally exhibit higher Nd (Fig. 8), Os and Pb isotope ratios (Fig. 9). Below, potential processes for generating the high-Nb group samples are discussed, including the role of subduction-fluids as well as the potential roles of enriched OIB-type mantle sources and slab and sediment melts.

### 5.3.1. Fluid enrichment

Relative enrichments in fluid mobile elements argue for a source with a subduction-fluid component, as for that of the low-Nb group source. Lower ratios of highly fluid mobile to less fluid mobile elements (e.g. Ba/La; Fig. 13) and lower  $^{87}\text{Sr}/^{86}\text{Sr}$  (Fig. 8) could be indicative of a lesser fluid flux relative to that of the low-Nb group source. Alternatively, such signatures could be an artifact of a less melt-depleted mantle wedge (e.g. higher Nb/Yb; Fig. 13) with higher concentrations of incompatible trace elements (thus less sensitive to fluid addition), or of lower degrees of partial melting of the source, which would also produce more incompatible element enriched melts. However, Pb/Ce ratios that are variable and higher than N-MORB cannot be explained by variable degrees of melting or variable source depletion, as these elements have identical partition coefficients during mantle melting and constant ratios in MORB and OIB (Hofmann et al., 1986). Rather, the positive correlation of Pb/Ce with Ba/La (Fig. 16) suggests that the high-Nb group source (low Pb/Ce) has received a lesser fluid flux than the low-Nb group source, a relationship seen commonly in arcs (e.g. Walker et al., 2000), and consistent with previous studies of the SCVF (Verma 1999; Marquez et al., 1999; LaGatta 2003).

The isotopic differences between the high-Nb and low-Nb group sources further argue for either isotopically distinct pre-subduction mantle wedge, or an isotopically distinct subduction-fluid component. The close match between the Pb isotope composition of the high-Nb group samples and local subducting hemi-pelagic sediment rather than pelagic sediment (Fig. 14) suggests that the source of the sediment-derived fluid component differs between the high-Nb and low-Nb group sources. Furthermore, it suggests that compared to the low-Nb group source, the Pb isotope composition of the high-Nb group source is even more strongly controlled by fluids derived from sediment relative to altered oceanic crust.

Note also that the negative correlations of Pb/Ce with  $^{206}\text{Pb}/^{204}\text{Pb}$  and  $^{187}\text{Os}/^{188}\text{Os}$  (Fig. 16b,c) are precisely opposite that expected for assimilation of upper crust or sediment, and argue further for a distinct mantle source for the high-Nb group samples.

### 5.3.2. *Intra-plate-type mantle*

The high-Nb group samples lack a significant negative Nb anomaly and are characterized by elevated HFSE and REE concentrations compared to the low-Nb group samples, observations potentially consistent with the involvement of an intra-plate or OIB-type mantle source, as has been previously proposed for the SCVF (e.g. Marquez et al., 1999). Such a model is consistent with the transitional intra-plate character of these samples on the ternary Pearce element discrimination diagram (Fig. 5). The negative correlation of Pb/Ce with Nb/U (Fig. 16d) and the OIB/MORB-like Nb/U ratio of the Xitle sample (00-00) is also consistent with such a model, given the much lower fluid mobility of U relative to Pb (Kogiso et al., 1997). However, the combined Sr-Nd-Pb isotope signatures do not correspond to any known OIB-type source (Fig. 17); Sr-Nd isotope compositions are similar to many E-MORB and some HIMU sources, whereas the Pb isotopes are similar only to extreme EMII OIB with very high  $\Delta 7/4$  values (Hofmann 2005). An OIB-type source can further be dismissed as a possible mixing end member based on trace element systematics, since none of the OIB end members serve as a satisfactory source to explain the Zr/Hf vs. Nb/Yb trend of the more enriched endmember group samples (Fig. 18).

### 5.3.3. *Slab Melting*

Eclogitic slab melts, such as those originally documented on Adak island, Aleutians (Kay 1978), could potentially impart the elevated HFSE and REE signatures that characterize the high-Nb group source, as these elements are highly incompatible during silicate melting. However, pure adakitic melts are characterized by relatively high Sr/Y ratios and low Y concentrations (Fig. 19) due to residual garnet in the eclogitic source (Defant and Drummond, 1990). Most of the samples from this study fall within the island arc range, and those from the high-Nb group exhibit the highest Y and lowest Sr/Y, indicating that they do not represent slab melts or mixtures of slab and mantle wedge melts (Fig. 19).

### 5.3.4. *Sediment Melting*

The high-Nb group samples could potentially reflect a component of subducted sediment melt, as such a melt could impart HFSE and REE enrichments to the mantle wedge. The overlap of Pb isotopic compositions of the high-Nb group samples with those of the subducting hemipelagic sediment (Fig. 14) is also consistent with such a model, as Pb will be effectively mobilized by both fluids and melts. The possibility of a sediment melt component in the source of the high-Nb group samples can be further evaluated via ratios of HFSE including Zr/Hf and Nb/Ta (Peate and Pearce, 1998). These ratios are not significantly fractionated from one another during mantle melting, resulting in most OIB and MORB having near chondritic ratios, yet residual trace phases (such as zircon and

rutile) that are potentially stabilized during sediment melting (Johnson and Plank, 1999) can strongly fractionate these elements.

Suprachondritic Zr/Hf ratios and a positive correlation with  $^{207}\text{Pb}/^{204}\text{Pb}$  (Fig. 20a) may therefore be indicative of a sediment melt contribution to the source. However, the elevated Zr/Hf ratios in the high-Nb group samples compared to the subducting hemipelagic sediment (Fig. 20a) argue that any sediment melt component cannot be a bulk melt. Rather, a residual trace phase that can fractionate the HFSE during melting would be required. The strongly suprachondritic Zr/Hf ratio of the more evolved endmember samples could be indicative of a sediment melt with residual zircon, as long as the melt composition is such that  $D_{\text{Hf}} > D_{\text{Zr}}$  (Linnen and Keppler, 2002; Tollstrup and Gill, 2005). Although the high-Nb group samples have approximately chondritic Nb/Ta ratios (Fig. 20b), a small increase in sediment Nb/Ta during melting with residual rutile (Foley et al., 2002; Schmidt et al., 2004; Tollstrup and Gill, 2005; Gomez-Tuena et al., 2007;) may result in relatively little modification of a MORB-like mantle wedge. The relatively low Nb/Ta ratios but more nearly chondritic Zr/Hf ratios in the low-Nb group samples may, in contrast, reflect the effect of residual amphibole during slab dehydration (Tiepolo et al., 2000).

These results lead to an inferred model (Fig. 21) in which the subducting Cocos plate releases hydrous fluids from both the pelagic sediment and altered oceanic lithosphere, causing melting and melt-depletion of the hydrated mantle wedge. Localized regions of the mantle wedge receive a subduction flux containing a component of hemipelagic sediment melt and lower fluid:melt ratio. The variable fluid:melt ratio may be a result of the lack of complete miscibility of fluid and melt during sediment dehydration and melting (Johnson and Plank, 1999), reflected on the small spatial scale of the SCVF. Alternatively, Patino et al. (2000) have proposed two other possible mechanisms to explain variable hydrous fluid:hemipelagic sediment melt ratios further south in Central America, including a physical model in which hemipelagic sediment distribution is controlled by horst and graben structures in the downgoing Cocos plate, and a two-stage metasomatic model in which a hemipelagic sediment melt infiltrates localized regions of the mantle wedge, which subsequently is fluxed by a hydrous fluid that results in melting of both the melt-infiltrated and barren regions of the wedge.

An alternative to these models, in which the high-Nb group source results from a veined pyroxenite source to which a small percent sediment melt has been added may alternatively explain the data (e.g. LaGatta, 2003). However, such a model would require that hemipelagic sediment melt be added only to the high-Nb veined source region and not the low-Nb source region, a phenomenon that cannot easily be explained.

#### *5.4. Implications for the Behavior of Os during Subduction*

The question of whether or not Os is mobile during subduction zone processes has been the source of significant recent controversy (e.g. Chesley et al., 2004). Studies of eclogites and blueschists thought to have experienced subduction dewatering suggest that Os is not significantly mobilized during subduction-related dehydration (Becker, 2000). Experimental studies have also generally suggested that Os mobility in hydrous fluids is relatively limited, although it may be slightly enhanced by oxidizing and/or saline fluid compositions (e.g. Xiong and Wood, 2000; Suzuki et al, 2003).

In contrast, several studies of mantle xenoliths from arc settings have documented Os isotope ratios higher than depleted MORB mantle (DMM;  $^{187}\text{Os}/^{188}\text{Os} = 0.122\text{-}0.127$ ; Snow and Reisberg, 1995) and even primitive upper mantle (PUM;  $^{187}\text{Os}/^{188}\text{Os} = 0.1296$ ; Meisel et al., 2001). Radiogenic Os isotope signatures in peridotites from the Cascades ( $^{187}\text{Os}/^{188}\text{Os} = 0.121\text{-}0.134$ ; Brandon et al., 1996), Japan ( $^{187}\text{Os}/^{188}\text{Os} = 0.124\text{-}0.130$ ; Brandon et al., 1996) and Kamchatka ( $^{187}\text{Os}/^{188}\text{Os} = 0.118\text{-}0.159$ ; Widom et al., 2003; Saha et al., 2005) all suggest that Os may be mobilized during subduction zone processes.

The origin of radiogenic Os isotope signatures in many arc lavas, including the Cascades (0.129 – 0.253; Borg et al., 2000) and Japan (0.136 – 0.205; Suzuki and Tatsumi, 2006) among many others (Alves et al., 2002), thus remains highly controversial (Chesley et al., 2004). The low Os abundances in most arc magmas (Alves et al., 2002) make them particularly susceptible to crustal assimilation, hence the cause of radiogenic Os signatures is often ambiguous. Previous Re-Os studies of the TMVB have concluded that radiogenic Os signatures are due to assimilation of lower crust (Lassiter and Luhr, 2001; Chesley et al., 2002). However, the results of the present study have demonstrated that neither lower nor upper crust assimilation can adequately account for the combined trace element and Sr, Nd, Pb and Os isotopic signatures of the SCVF lavas. Rather, the correlation of Os isotopes with trace element and Pb isotope signatures imparted by subduction-related metasomatism of the mantle wedge suggest that the radiogenic Os in these samples also may be attributed to such processes.

The hyperbolic curvature of the data trends on plots such as  $^{187}\text{Os}/^{188}\text{Os}$  vs.  $^{206}\text{Pb}/^{204}\text{Pb}$  (Fig. 10) and  $^{187}\text{Os}/^{188}\text{Os}$  vs. Ba/Zr (Fig. 22) can be interpreted as two-component mixing trends in which the magmas represent melts of variable proportions of two compositionally and isotopically distinct mantle sources. The low-Nb group samples are characterized by less radiogenic Os, but all samples are more radiogenic than DMM and PUM, consistent with subduction components that contain significant radiogenic Os. The relatively strong curvature allows some constraints to be placed on the compositions of the mixing endmembers, and suggests that the low-Nb group source likely has a  $^{187}\text{Os}/^{188}\text{Os}$  close to but  $<0.133$ , as represented by the Jorullo sample. The high-Nb group source, thought to be generated from a depleted mantle wedge fluxed by hydrous fluids as well as melt from hemipelagic sediment, has a  $^{187}\text{Os}/^{188}\text{Os}$  ratio  $>0.261$ .

The source of radiogenic Os could be either the subducted altered oceanic crust or sediment, as both will be characterized by radiogenic Os. However, oceanic crust typically has very low Os abundances (low ppt range; Gannoun et al., 2004) and young oceanic crust such as the ~15 Ma Cocos plate will likely have  $^{187}\text{Os}/^{188}\text{Os} < \sim 0.4$ , assuming typical  $^{187}\text{Re}/^{188}\text{Os}$  ratios of ~1,000 (Gannoun et al., 2004; Suzuki and Tatsumi, 2006). In contrast, marine sediment generally has higher Os abundances (~30 – 1,000 ppt; Peucker-Ehrenbrink et al., 1995; Suzuki and Tatsumi, 2006) and substantially higher  $^{187}\text{Os}/^{188}\text{Os}$  of ~1.0 or higher (Peucker-Ehrenbrink et al., 1995). Therefore, marine sediment will have substantially more leverage in overprinting the Os isotopic signature of the mantle wedge, which likely has Os abundances of several ppb as typical of normal mantle peridotite. The more radiogenic Os isotope signature associated with the more enriched source further suggests that sediment melt may be a more effective metasomatic agent than hydrous fluid in the case of Os. This conclusion is similar to that of a study of mantle xenoliths in Kamchatka (Widom et al., 2003), where it was suggested that dehydration of an older (~100 Ma) and colder slab in southern Kamchatka led to less

radiogenic Os isotope signatures imparted to the mantle wedge compared to that produced by melts of the younger (~15-25 Ma) and hotter slab in the north. In either case, the relatively radiogenic Os isotope signatures of both endmember sources contributing to SCVF volcanism require high Os abundances in the respective fluids and melts, and/or very high fluid:rock ratios during subduction metasomatism.

## 6. Conclusion

Chemical and isotopic variations in mafic magmas of the SCVF suggest that there are two different compositional endmembers that can be distinguished based on the magnitude of their Nb-anomalies. One endmember (the “low-Nb” endmember) has a strong negative Nb anomaly similar to typical arc magmas, whereas the other endmember (the “high-Nb” endmember) lacks a strong negative Nb anomaly, and as such shares some compositional characteristics with intra-plate type magmas.

Trace element and isotopic variations of the SCVF lavas argue against an important role for either lower or upper crustal assimilation. Although the lavas are all more radiogenic in Os than MORB mantle or PUM, the positive correlation of  $^{187}\text{Os}/^{188}\text{Os}$  with  $^{206}\text{Pb}/^{204}\text{Pb}$  argues against a significant role for lower crustal assimilation. Negative correlations of Pb/Ce with both  $^{187}\text{Os}/^{188}\text{Os}$  with  $^{206}\text{Pb}/^{204}\text{Pb}$  further argue against a significant role for either upper or lower crustal assimilation.

Rather, the data are best explained by mixing of mantle sources that have been variably affected by subduction processes. All samples exhibit enrichments in fluid mobile elements (Cs, Ba, K, Pb and Sr) suggestive of derivation from a mantle wedge that has been fluxed with hydrous subduction fluids, and variations in Pb isotope ratios that mimic those of the local subducting sediment suggest that the fluids/melts are derived from both the altered oceanic crust and sediment. Relatively high Ba/La and low Nb/Yb ratios, and the strong negative Nb anomaly in the low-Nb group SCVF lavas suggest that they result from melting of a depleted mantle source that has been fluxed with hydrous fluid. The high-Nb group lavas are generated from similar mantle wedge that was infiltrated by an additional subduction component. High Zr/Hf ratios but near chondritic Nb/Ta ratios, as well as high  $^{207}\text{Pb}/^{204}\text{Pb}$  and  $\Delta 7/4$  in the high-Nb group lavas may reflect derivation from a mantle wedge that has been influxed with a hemipelagic sediment melt produced in the presence of residual zircon.

Os isotope signatures in the SCVF lavas are all more radiogenic than PUM despite the evidence against a role for either upper or lower crustal assimilation, and furthermore appear to reflect the different modes of subduction metasomatism of the mantle wedge. Relatively less radiogenic signatures ( $^{187}\text{Os}/^{188}\text{Os} \sim 0.133$ ) characterize mantle wedge that has been fluxed with hydrous fluid, whereas mantle wedge that has been metasomatized with a sediment melt has more extreme Os isotopic signatures ( $^{187}\text{Os}/^{188}\text{Os} > 0.26$ ). These results suggest that radiogenic Os is mobilized during subduction zone processes, and require high Os abundances in the metasomatic fluids/melts and/or very high fluid:rock ratios.

Table 1. Major and trace element data (grouped by wt% MgO). Major elements are in wt%, trace elements in ppm.

	*B3-06	*PG05-16	*PG05-18	JOR-0611	*96365	00-00	*PG05-19	*96358	PO 0569
SiO <sub>2</sub>	52.50	53.12	53.26	51.81	54.58	51.50	53.62	56.59	53.28
TiO <sub>2</sub>	1.22	0.79	0.85	0.78	0.80	1.89	1.25	1.00	1.67
Al <sub>2</sub> O <sub>3</sub>	14.82	15.21	15.43	16.05	15.52	16.40	15.64	14.78	16.43
Fe <sub>2</sub> O <sub>3</sub>	8.48	7.95	7.86	8.06	7.90	10.14	8.11	6.97	9.31
MnO	0.13	0.12	0.12	0.12	0.13	0.16	0.12	0.10	0.13
MgO	10.11	10.09	9.78	9.35	9.23	8.68	8.44	8.13	7.78
CaO	7.85	7.95	7.64	8.37	7.80	8.18	7.35	6.89	7.69
Na <sub>2</sub> O	3.56	3.32	3.41	3.28	3.26	3.75	3.56	3.53	3.86
K <sub>2</sub> O	1.11	0.91	0.92	0.74	0.99	0.92	1.15	1.19	0.92
P <sub>2</sub> O <sub>5</sub>	0.30	0.15	0.17	0.15	0.17	0.51	0.24	0.23	0.42
LOI	0.09	0.14	<0.01	-0.09	0.09	-0.34	<0.01	0.52	-0.25
	B3-06	PG05-16	PG05-18	JOR-0611	96365	00-00	PG05-19	96358	PO 0569
Li	9	12	11	10	12	10	12	13	11
Be	1	1	1	1	1	2	1	1	2
Sc	22	18	25	27	22	23	24	19	24
V	146	144	171	166	151	170	156	126	166
Cr	404	501	573	549	547	346	356	363	302
Co	45	36	43	45	39	42	41	33	38
Ni	289	215	293	271	239	176	220	198	161
Cu	37	42	42	64	42	38	41	29	32
Zn	73	66	79	75	70	84	75	70	86
Ga	18	16	20	18	17	18	18	19	19
Rb	17	20	21	13	20	19	21	28	21
Sr	486	338	437	400	356	516	418	497	465
Y	23	17	21	17	18	33	24	21	29
Zr	158	105	138	96	118	242	170	165	226
Nb	11	4	4	2	4	19	12	8	15
Mo	1	0.5	0.7	0.5	0.7	2	0.9	1	1
Cs	0.5	0.8	0.8	0.4	0.9	0.5	0.7	1	0.6
Ba	247	207	248	216	225	279	234	308	273
La	14	9	11	7	10	21	13	15	18
Ce	32	22	26	18	24	46	30	33	40
Pr	4	3	4	2	3	6	4	4	5
Nd	18	12	15	10	14	26	17	18	23
Sm	4	3	3	3	3	6	4	4	5
Eu	1	0.9	1	1	1	2	1	1	2
Gd	4	3	3	3	3	6	4	4	5
Tb	0.6	0.5	0.6	0.4	0.5	0.8	0.6	0.6	0.7
Dy	4	3	3	3	3	5	4	3	4
Ho	0.8	0.6	0.7	0.6	0.6	1	0.8	0.7	0.9
Er	2	1	2	1	2	3	2	2	2
Tm	0.3	0.2	0.3	0.2	0.3	0.4	0.3	0.3	0.3
Yb	2	1	2	1	2	3	2	2	2
Lu	0.3	0.2	0.2	0.2	0.2	0.4	0.3	0.2	0.3
Hf	3	2	3	2	3	4	3	4	4
Ta	0.8	0.5	0.5	0.3	1	1	1	1	0.8
Pb	4	3	5	4	4	4	4	5	4
Th	1	0.8	1	-	1	2	1	2	1
U	0.3	0.2	0.3	-	0.3	0.4	0.3	0.6	0.4

\* are from UNAM

Table 1. Continued

	TPTZ07-01A	CH06-01	CL-0701
SiO <sub>2</sub>	62.49	99.49	0.00
TiO <sub>2</sub>	0.73	0.01	0.02
Al <sub>2</sub> O <sub>3</sub>	16.41	0	0.27
Fe <sub>2</sub> O <sub>3</sub>	5.28	1.19	0.27
MnO	0.09	0.06	0.01
MgO	3.35	0.6	0.57
CaO	5.55	0.22	53.48
Na <sub>2</sub> O	3.89	0	0
K <sub>2</sub> O	1.35	0.01	0.26
P <sub>2</sub> O <sub>5</sub>	0.18	0.04	0.02
LOI	1.28	0.11	42.99
	TPTZ07-01A	CH06-01	#CL-0701
Li	8	2	
Be	2	0.1	
Sc	14	0.2	1
V	126	13	2
Cr	96	8	
Co	18	0.8	
Ni	46	7	2
Cu	20	9	1
Zn	66	18	8
Ga	22	0.7	
Rb	20	2	3
Sr	424	14	307
Y	19	2	5
Zr	143	2	-
Nb	4	0.3	
Mo	0.7	0.1	
Cs	0.5	0.1	
Ba	250	14	2
La	11	0.7	
Ce	19	3	
Pr	3	-	
Nd	14	0.3	
Sm	3	0.1	
Eu	1	0.1	
Gd	3	0.1	
Tb	0.5	0.1	
Dy	3	0.6	
Ho	0.6	0.2	
Er	2	0.4	
Tm	0.3	0.1	
Yb	2	0.3	
Lu	0.2	0.1	
Hf	3	0	
Ta	2	0	
Pb	5	2	
Th	0.8	-	
U	0.3	-	

# indicates DCP analyses

Table 2. Isotope data for whole rock samples from the SCVF and Jorullo.

Isotopes	B3-06	PG05-16	PG05-18	JOR-0611	96365	00-00	PG05-19	96358	PO 0569	TPT207-01A	CH06-01	CL-0701
$^{87}\text{Sr}/^{86}\text{Sr}$	0.703610	0.704160	0.703995	0.703925	0.704186	0.703602	0.703629	0.704015	0.703801 0.703818	0.703684 0.703664	0.71213	0.7073
$^{143}\text{Nd}/^{144}\text{Nd}$	0.512932	0.512831	0.512861	0.512832	0.512817	0.512855	0.512892	0.512823	0.512814 0.512802	0.512890 0.512895	0.51242	none
$^{206}\text{Pb}/^{204}\text{Pb}$	18.6472	18.6888	18.6509	18.6337	18.6776	18.7481	18.7074	18.6935	18.7590 18.7455	18.5962 18.5952	18.7483	22.2874
$^{207}\text{Pb}/^{204}\text{Pb}$	15.5818	15.5923	15.5716	15.5823	15.5789	15.6440	15.5935	15.6159	15.6130 15.5958	15.5562 15.5548	15.6621	15.8125
$^{208}\text{Pb}/^{204}\text{Pb}$	38.3625	38.4531	38.3625	38.3673	38.4177	38.4751	38.4529	38.5001	38.5320 38.4767	38.2507 38.2457	38.8003	38.8634
$^{187}\text{Os}/^{188}\text{Os}$	0.1447 0.1635	0.1440 0.1564	0.1410	0.1329	0.1653	0.2235	0.1589	0.1498	0.2608	0.2422	0.4735	1.1798
Concentrations												
Os (ppb)	0.125 0.070	0.075 0.052	0.150	0.082	0.067	0.028	0.056	0.065	0.012	0.011	0.002	0.019
Re (ppb)	0.039 0.032	0.076 0.062	0.080	0.090	0.045	-	0.093	0.029	0.066	0.032	0.008	0.235
$^{187}\text{Re}/^{188}\text{Os}$	1.536 2.245	4.900 5.774	2.579	5.294	3.251	-	7.980	2.112	28.648	13.987	19.006	68.149

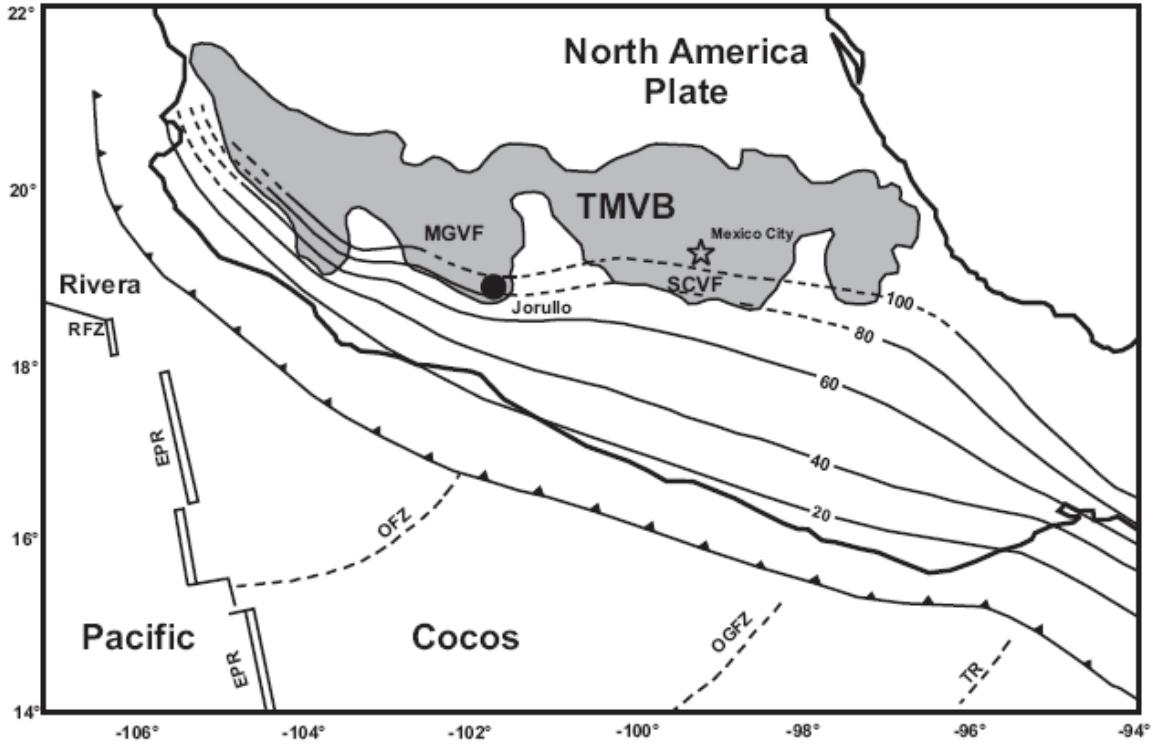


Figure 1 (from Pardo and Suarez, 1995). Map of the TMVB. The TMVB (gray field) is located on the North America Plate, beneath which the Rivera and Cocos plates are subducting at the Middle-American trench.

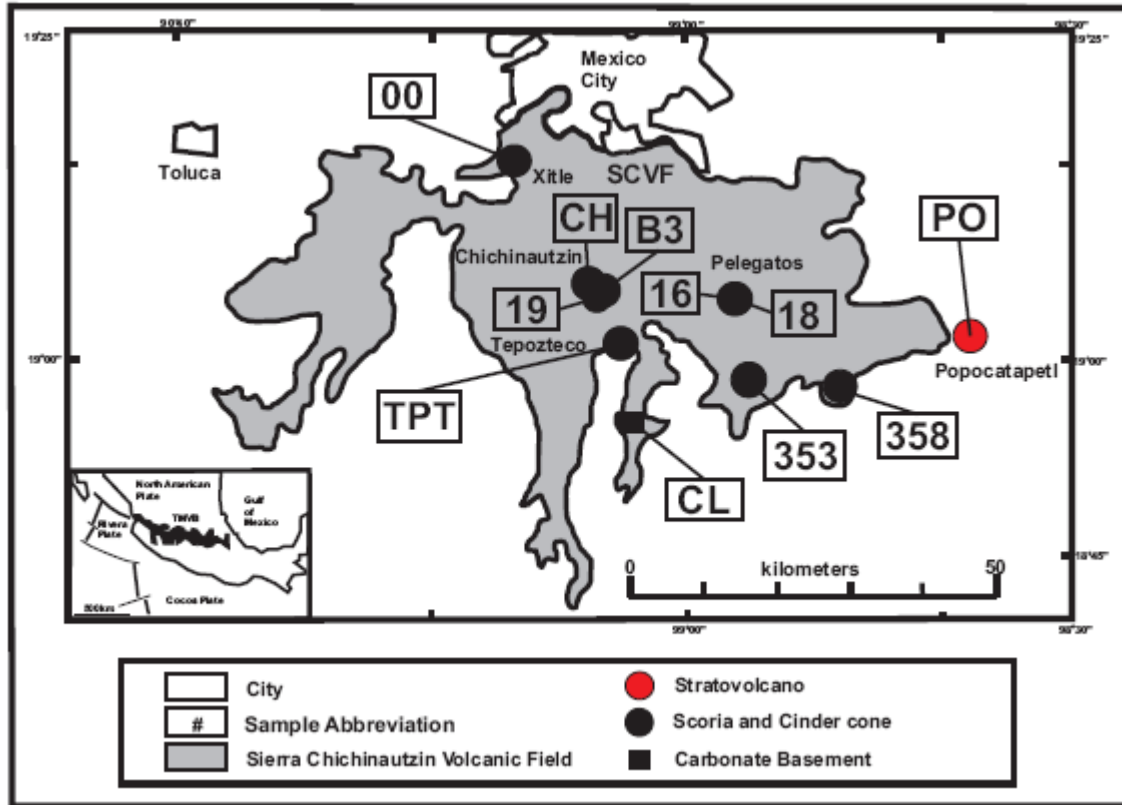


Figure 2 (after Siebe et al., 2004). Map of the Sierra Chichinautzin Volcanic Field, showing active volcanoes including stratovolcanoes (red) and scoria cones (black). Sample locations are marked with abbreviated sample numbers as follows: 00=00-00; CH=CH06-01; B3=B3-06; PO=PO 0569; 16=PG05-16; 18=PG05-18; 19=PG05-19; TPT=TPTZ07-01A; CL=CL07-01; 353=96353; 358=96358.

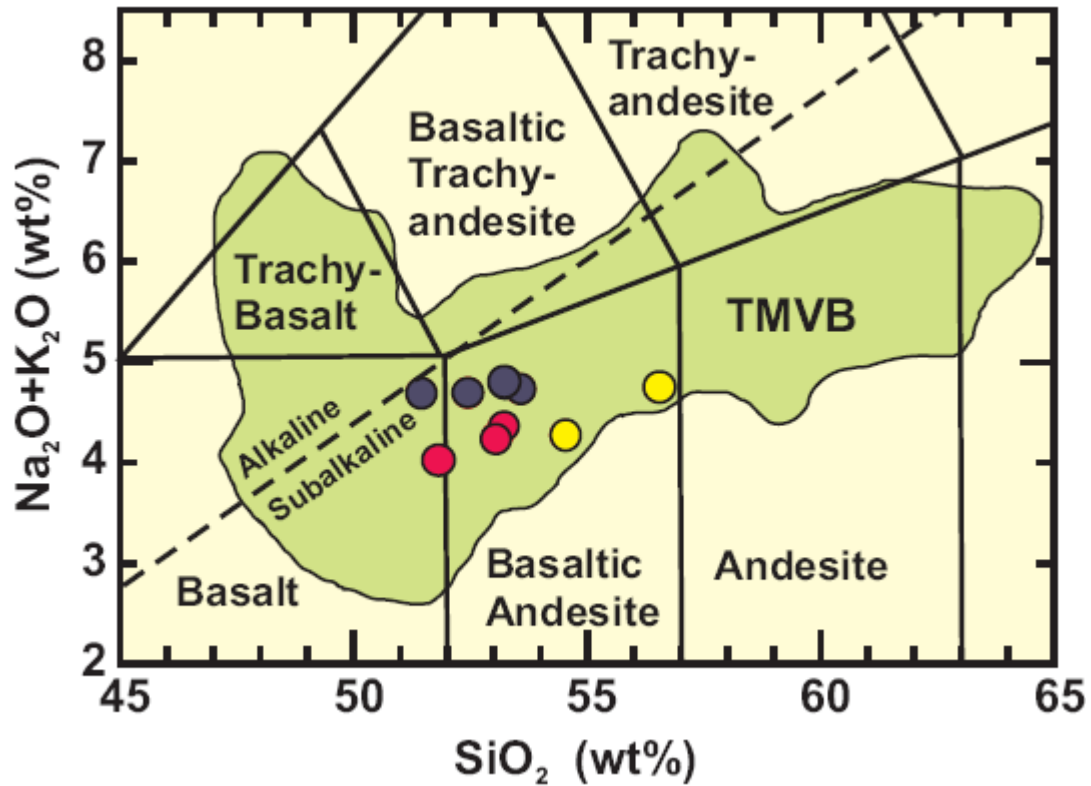


Figure 3 (after LeBas et al., 1986). Alkalis vs. silica classification diagram. All samples from this study fall within the subalkaline basalt and basaltic andesite fields. The green field represents the range of rocks of the TMVB (data from Lassiter and Luhr, 2001; Chesley et al., 2002; Siebe et al., 2004; Ferrari et al., 2000; Schaaf et al., 2005). In this and subsequent figures, the SCVF lavas are color coded based the magnitude of their Nb-anomalies as illustrated in Fig. 6 (blue = high-Nb group samples; red = low-Nb group samples; yellow =intermediate composition samples).

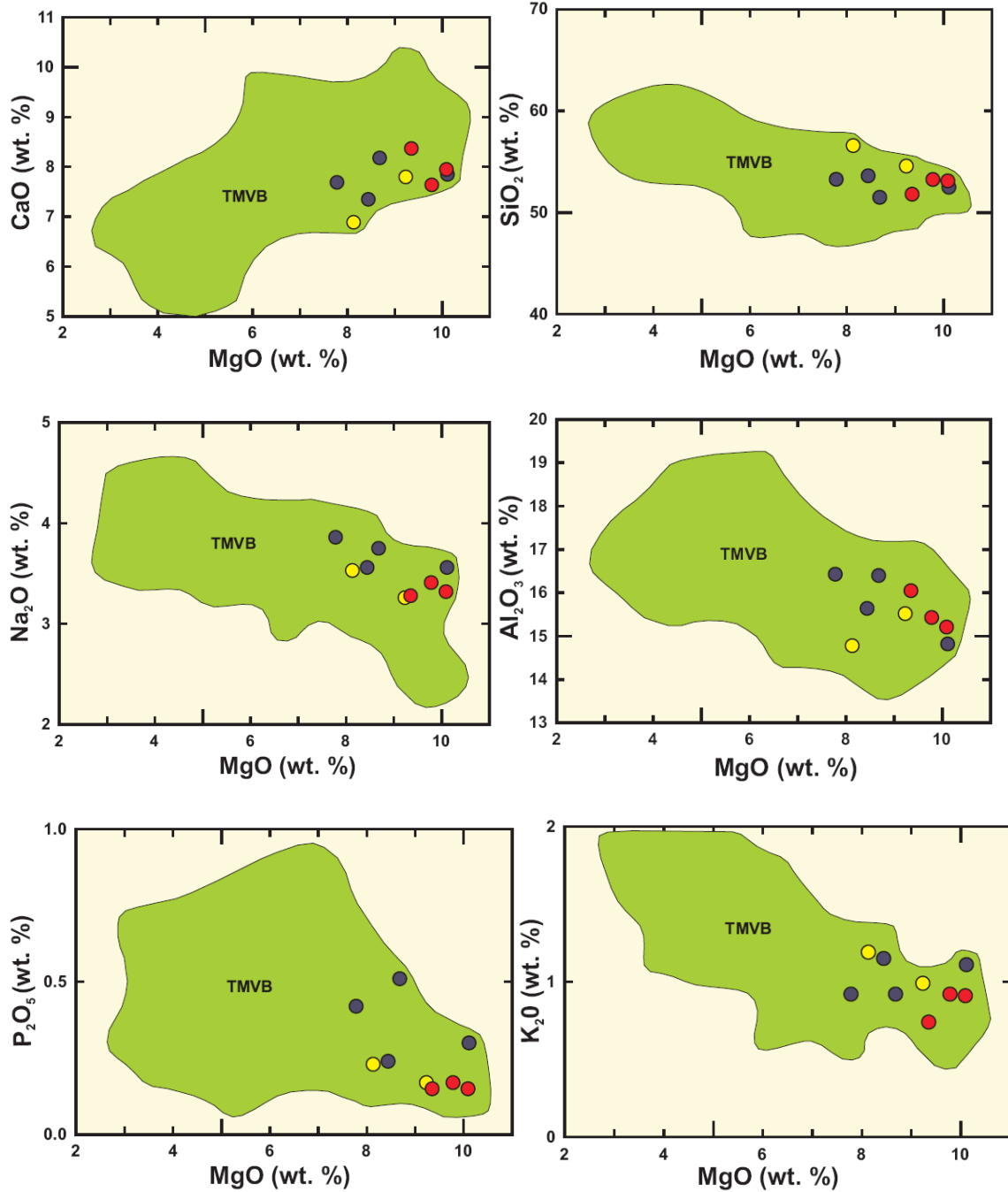


Figure 4. Harker diagrams showing major element concentrations vs. MgO for SCVF lavas. All samples fall within the broader TMVB field (green). TMVB data from Siebe et al., 2004; Ferrari et al., 2000; Lassiter and Luhr, 2001; Chesley et al., 2002.

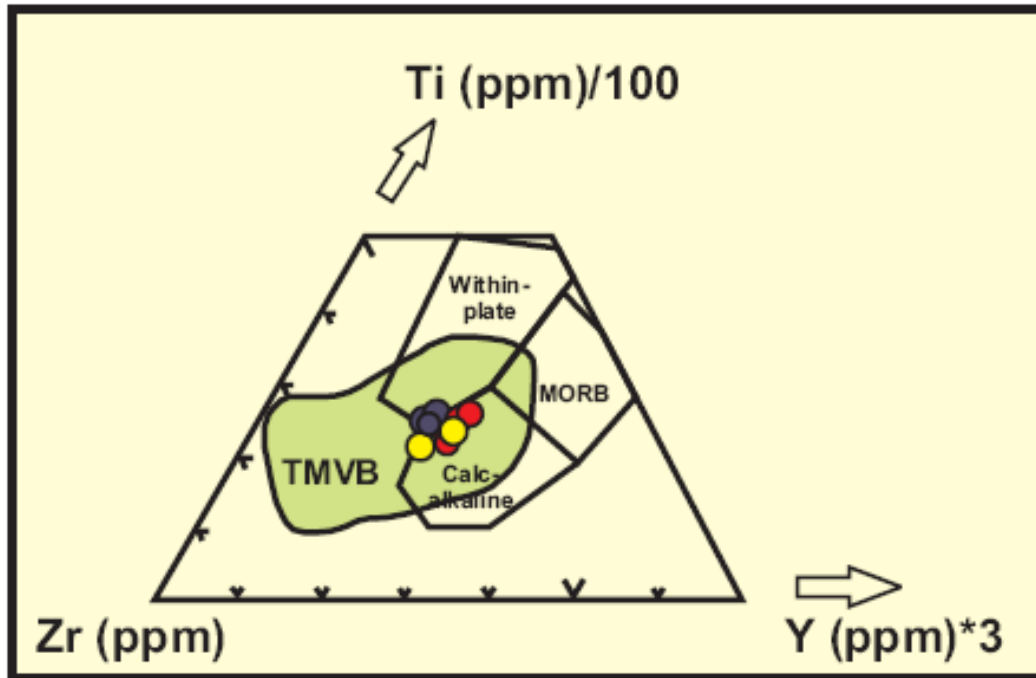


Figure 5. Pearce element discrimination diagram ( $Zr-Ti/100-Y*3$ ) showing the SCVF lavas and the broader TMVB field (green; data from Siebe et al., 2004; Ferrari et al., 2000). Samples from this study are mostly calc-alkaline, with a few transitional with the intra-plate field.

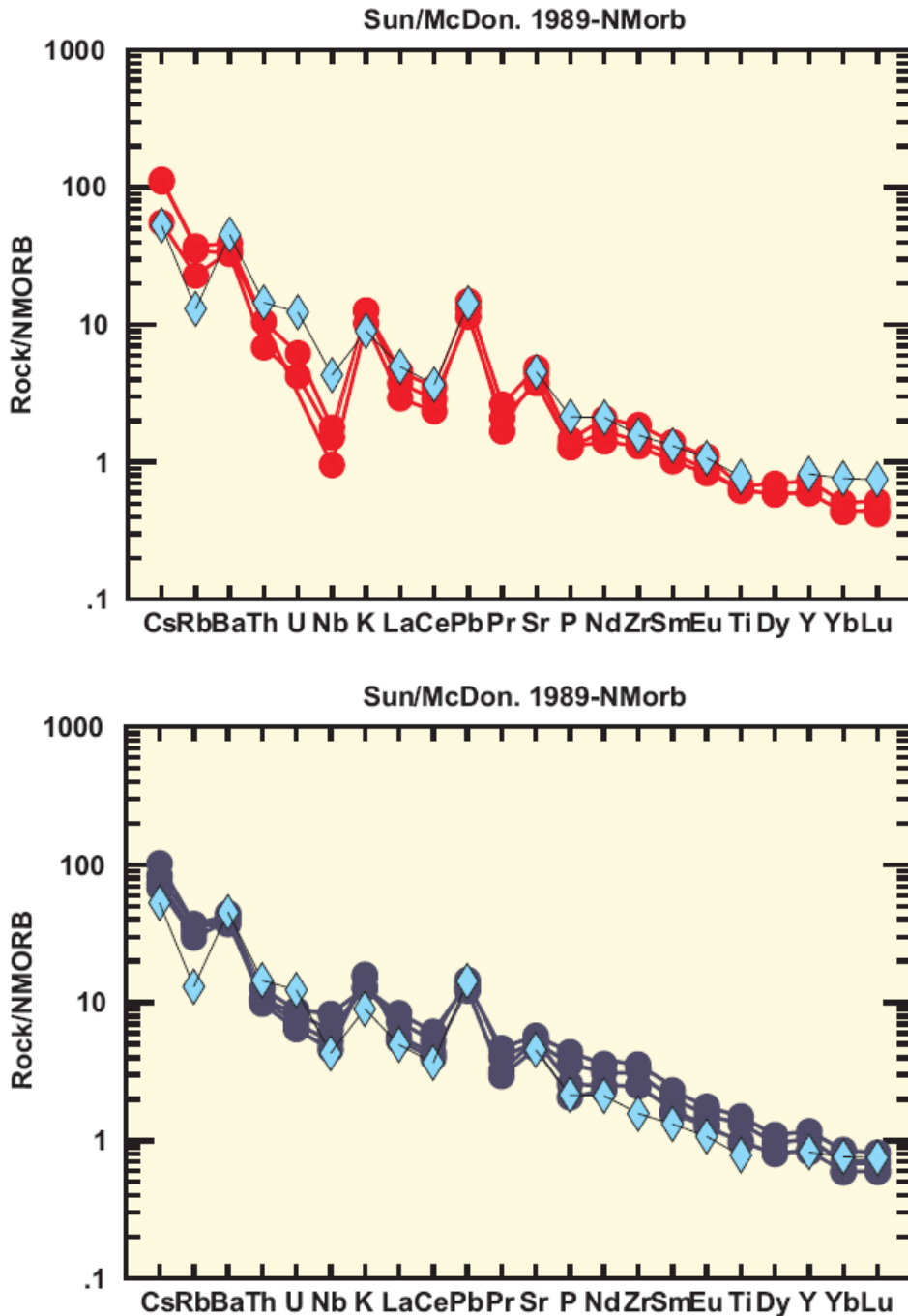


Figure 6. N-MORB-normalized trace element diagram showing two groups of SCVF lavas including (a) the “low-Nb” group with distinctive negative Nb-anomalies (JOR-0611, PG05-16, and PG05-18) and (b) the “high-Nb” group samples that lack strong negative Nb anomalies (B3-06, 00-00, PO 0569, and PG05-19). Light blue diamonds represent typical arc lavas with hydrous fluid signatures (Borg et al., 2000). The two SCVF sample groups are referred to in this paper, respectively, as the “less enriched endmember” and “more enriched endmember” groups.

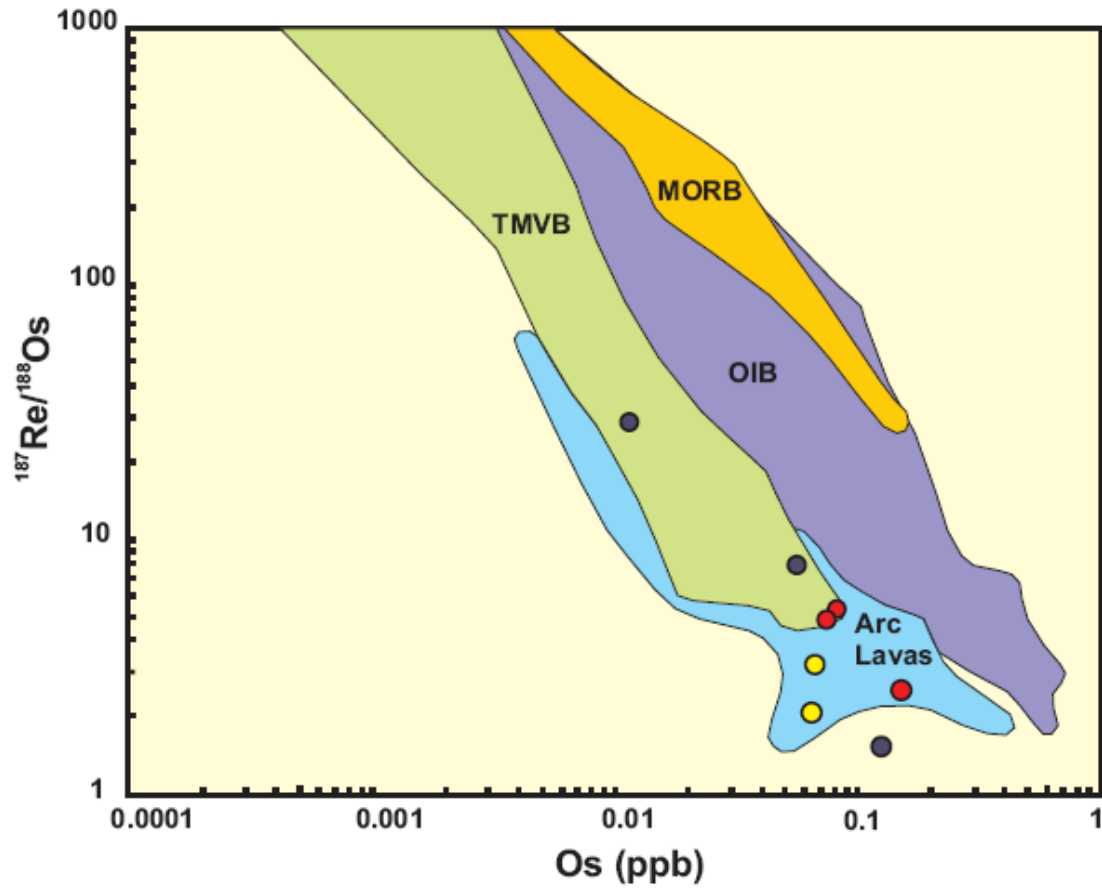


Figure 7.  $^{187}\text{Re}/^{188}\text{Os}$  versus Os concentration for SCVF lavas compared to fields for the TMVB, OIB (ocean island basalts), MORB (mid-oceanic ridge basalts), and arc lavas. The SCVF lavas are similar to other arc lavas in having low Re/Os ratios for a given Os concentration relative to MORB and OIB (literature data from Chesley et al., 2002; Alves et al., 2002; Borg et al., 2000; Gannoun et al., 2007; Hauri and Hart, 1993; and Reisberg et al., 1993.)

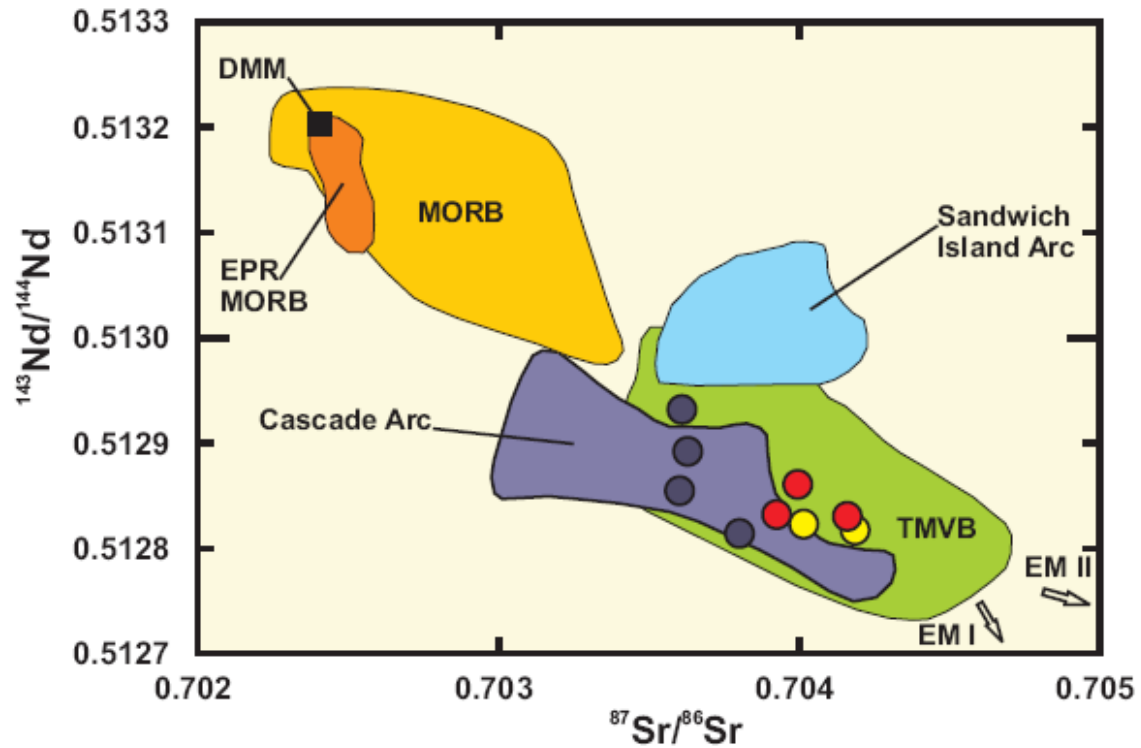


Figure 8 (after Tatsumi, 2005).  $^{143}\text{Nd}/^{144}\text{Nd}$  versus  $^{87}\text{Sr}/^{86}\text{Sr}$  for SCVF lavas compared to other samples from the TMVB (green field), MORB and EPR (yellow fields), and other arcs (blue fields). Literature data from the following sources: TMVB (Valdez-Moreno et al., 2006; Siebe et al., 2004; and Schaaf et al., 2005); MORB and EPR (Ito et al., 1987); Cascades (Borg et al., 2000); Sandwich island arc (Pearce et al., 1995).

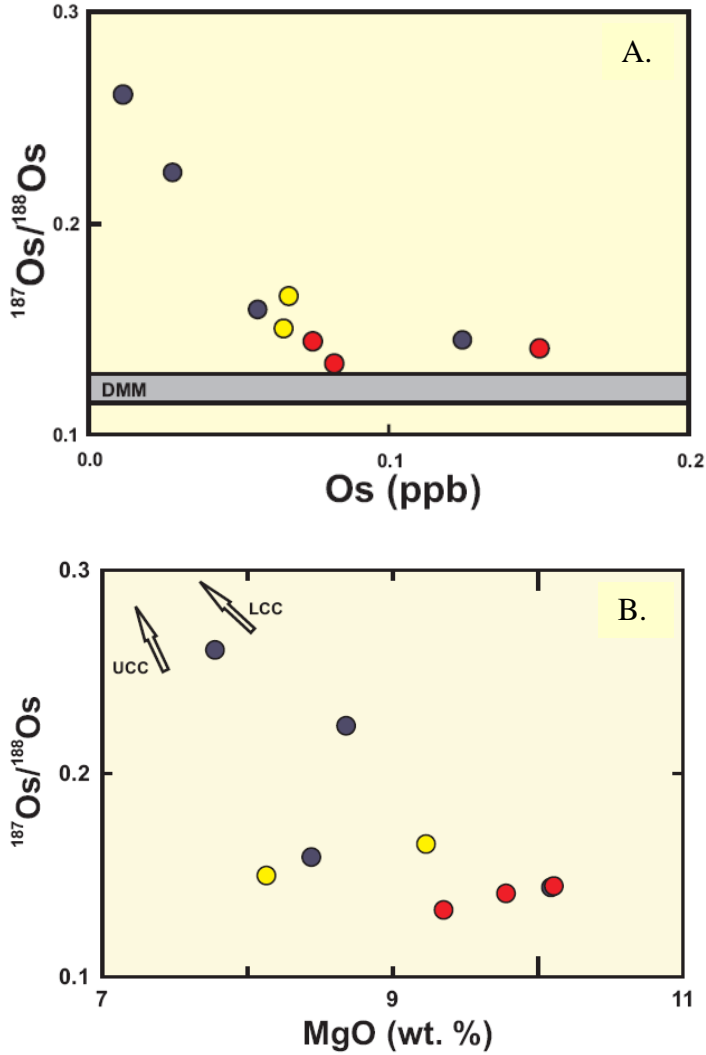


Figure 9. (a)  $^{187}\text{Os}/^{188}\text{Os}$  versus Os concentration. The gray band shows the Os isotope range of DMM (depleted MORB mantle) based on abyssal peridotites (Snow and Reisberg, 1995). (b)  $^{187}\text{Os}/^{188}\text{Os}$  versus MgO. The negative correlations between  $^{187}\text{Os}/^{188}\text{Os}$  and Os and MgO concentrations could be due to either crustal assimilation or subduction-fluid metasomatism, as both could impart radiogenic crustal Os signatures to the lavas (arrows to upper and lower crust based on values of Rudnick and Gao, 2003.)

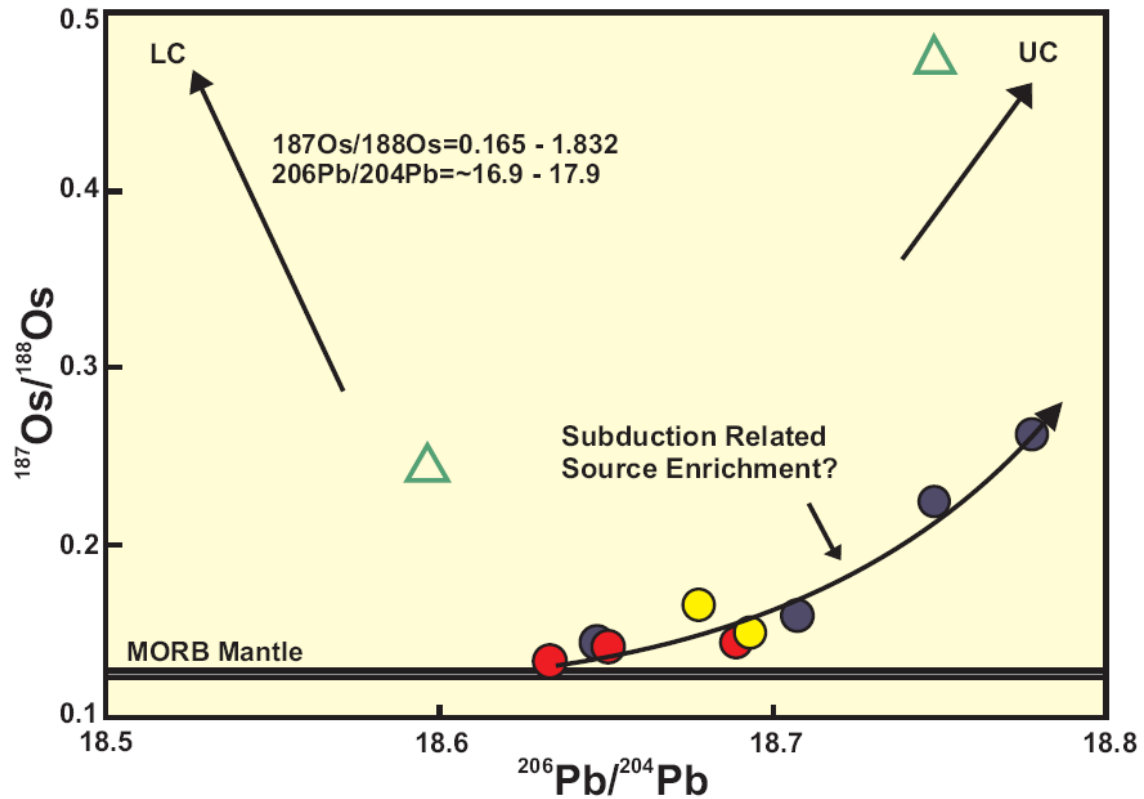


Figure 10.  $^{187}\text{Os}/^{188}\text{Os}$  versus  $^{206}\text{Pb}/^{204}\text{Pb}$ , showing range for SCVF lavas and the compositions of the quartz-rich cumulate and andesite xenolith from this study. The positive correlation of the SCVF lavas is inconsistent with assimilation of lower crust, but could be consistent with assimilation of upper crust (upper and lower crustal values are from Rudnick and Gao, 2003; Mexican lower crustal Pb isotope values from LaGatta, 2003; Os isotope ratios for lower crust of other localities from Saal et al., 1998 and Esperanca et al., 1997; DMM Pb isotope range from Ito et al., 1987 and Os isotope range from Snow and Reisberg, 1995).

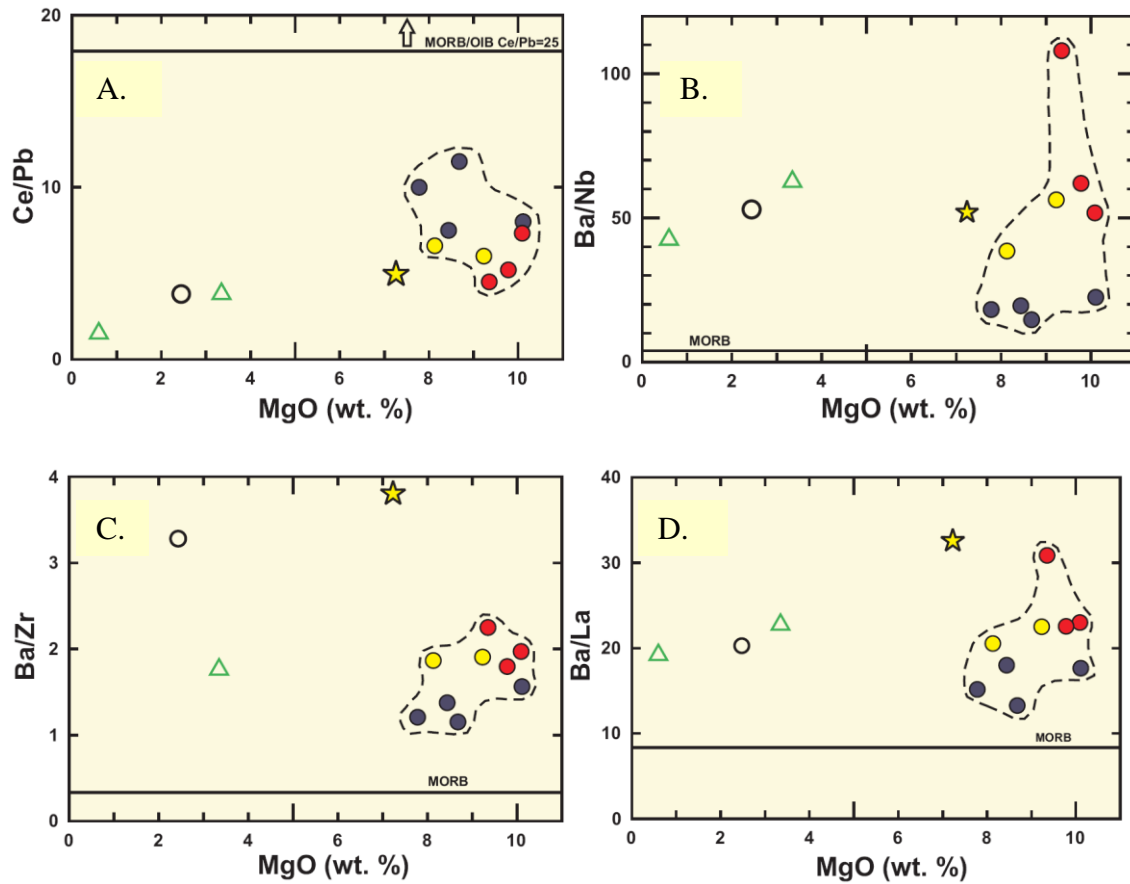


Figure 11. Trace element ratios versus MgO (wt%) for SCVF lavas and average lower crust ( star) and upper crust (black circle). Green triangles are quartz-rich cumulate and andesitic xenoliths from this study. MORB values are indicated by gold boxes. (Crustal and MORB data from Rudnick and Gao, 2003; Hofmann et al., 1986; Sun and McDonough, 1989).

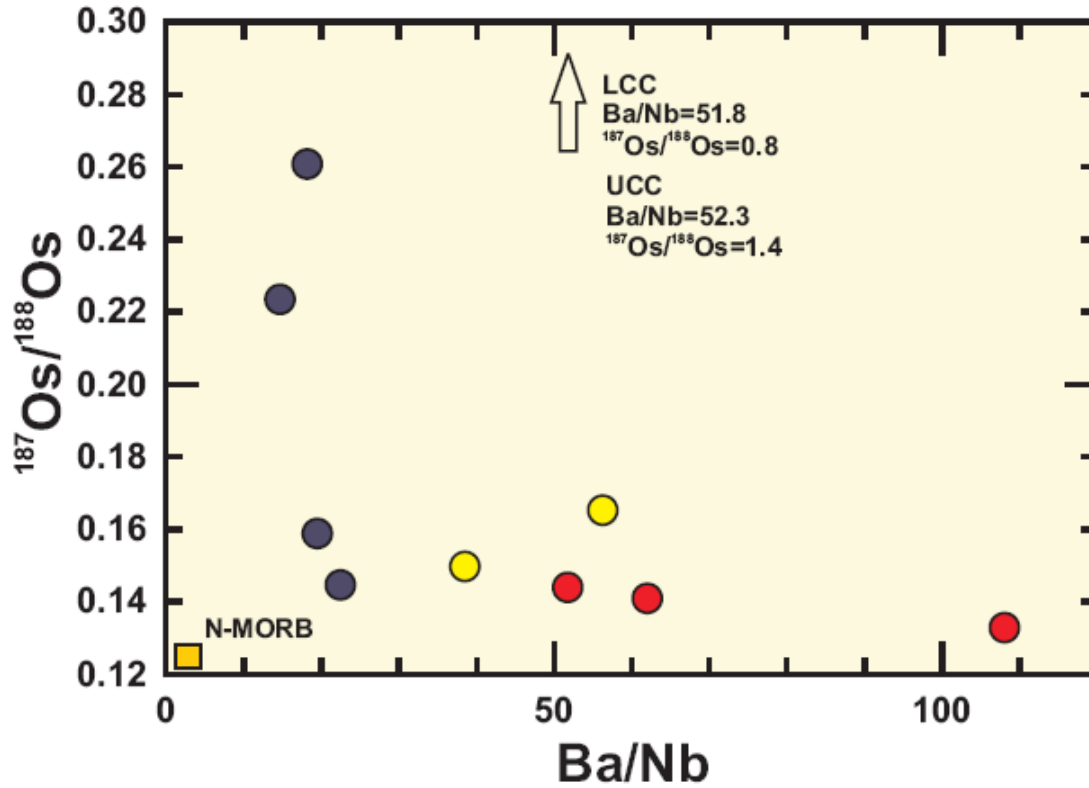


Figure 12.  $^{187}\text{Os}/^{188}\text{Os}$  versus Ba/Nb for SCVF lavas and average upper and lower crust (crustal and MORB data from Rudnick and Gao, 2003; Hofmann et al., 1986; Sun and McDonough, 1989; Snow and Reisberg, 1995). Symbols as in Fig. 11.

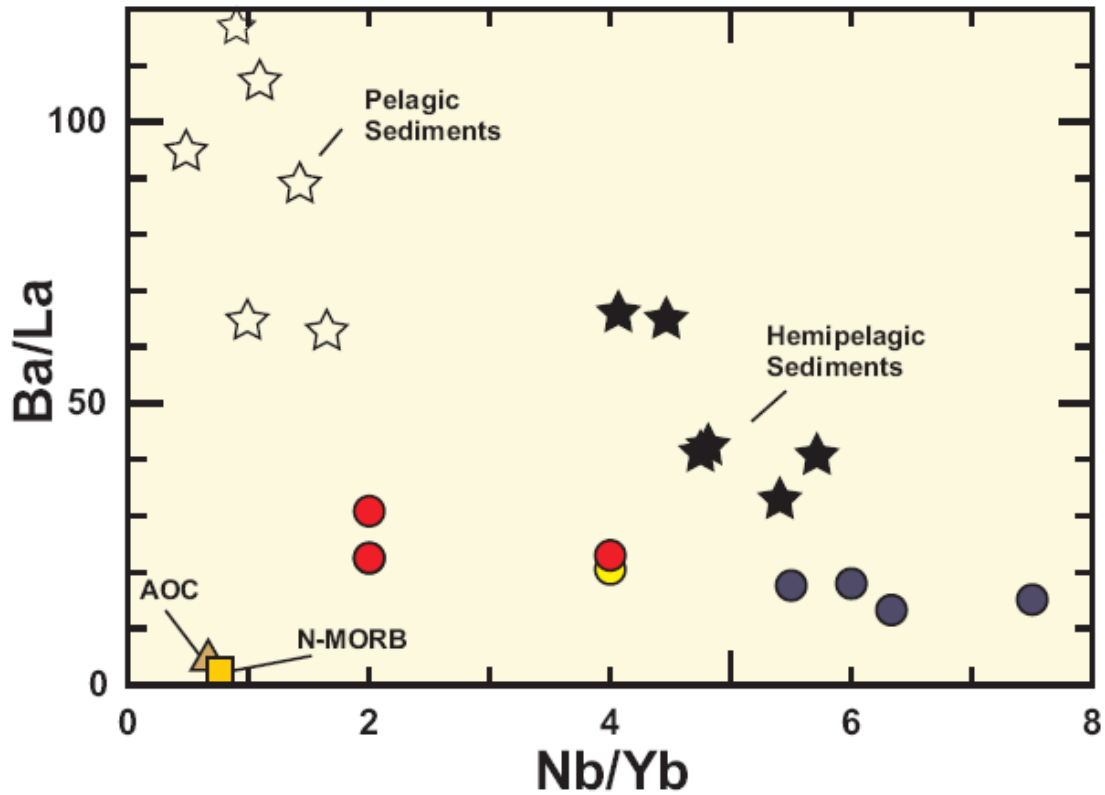


Figure 13. Ba/La versus Nb/Yb showing range for SCVF lavas in comparison to N-MORB (gold box), altered oceanic crust (AOC; filled triangle) and Mexican subducting sediment from DSDP 487 (filled stars are hemipelagic sediments, open stars are pelagic sediments). (Sediment, AOC, and N-MORB data from LaGatta, 2003; Gomez-Tuena et al., 2007; Sun and McDonough, 1989).

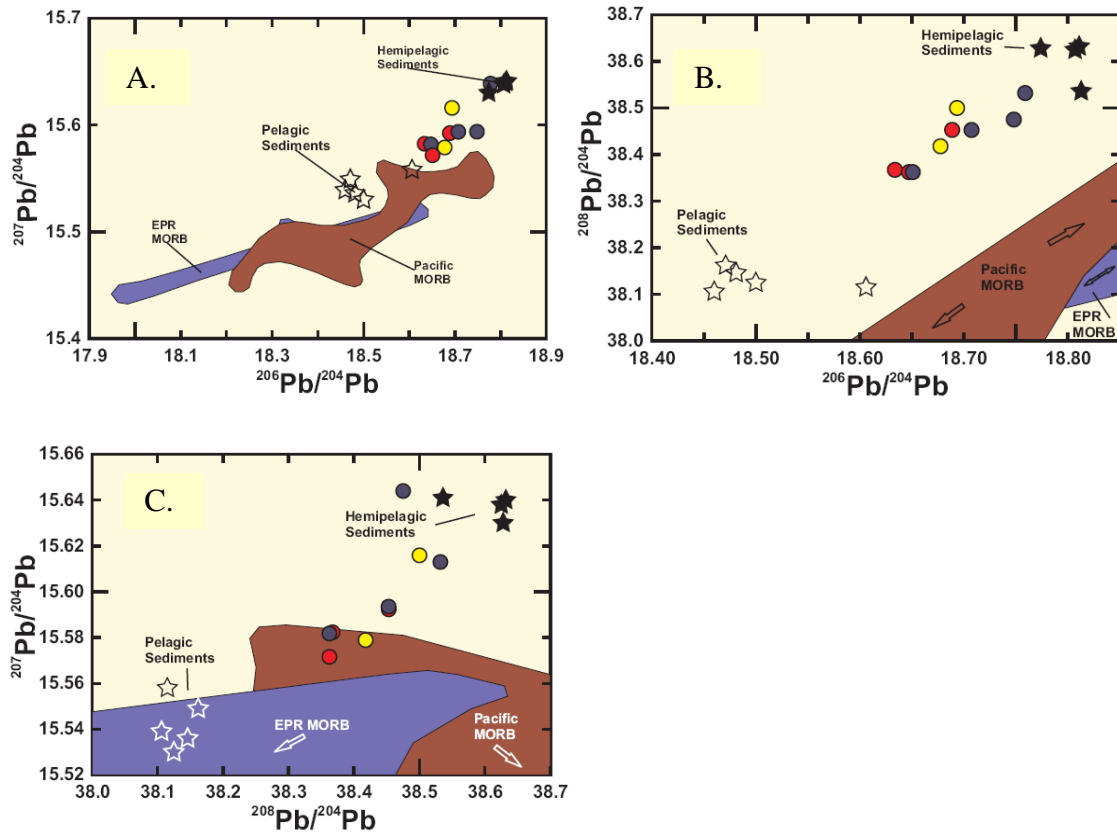


Figure 14. (a)  $^{207}\text{Pb}/^{204}\text{Pb}$  vs.  $^{206}\text{Pb}/^{204}\text{Pb}$ , (b)  $^{208}\text{Pb}/^{204}\text{Pb}$  vs.  $^{206}\text{Pb}/^{204}\text{Pb}$ , and (c)  $^{207}\text{Pb}/^{204}\text{Pb}$  vs.  $^{208}\text{Pb}/^{204}\text{Pb}$  variations in SCVF lavas compared to ranges for Pacific MORB (rust-colored field), EPR MORB (light blue field) and Mexican sediment (symbols as in Fig. 13). The SCVF lavas exhibit Pb isotope ranges that are closely bracketed by the hemipelagic and pelagic sediment values, suggesting a significant sediment Pb contribution to the lavas. MORB data are from Ito et al., (1987); sediment data are from LaGatta, (2003).

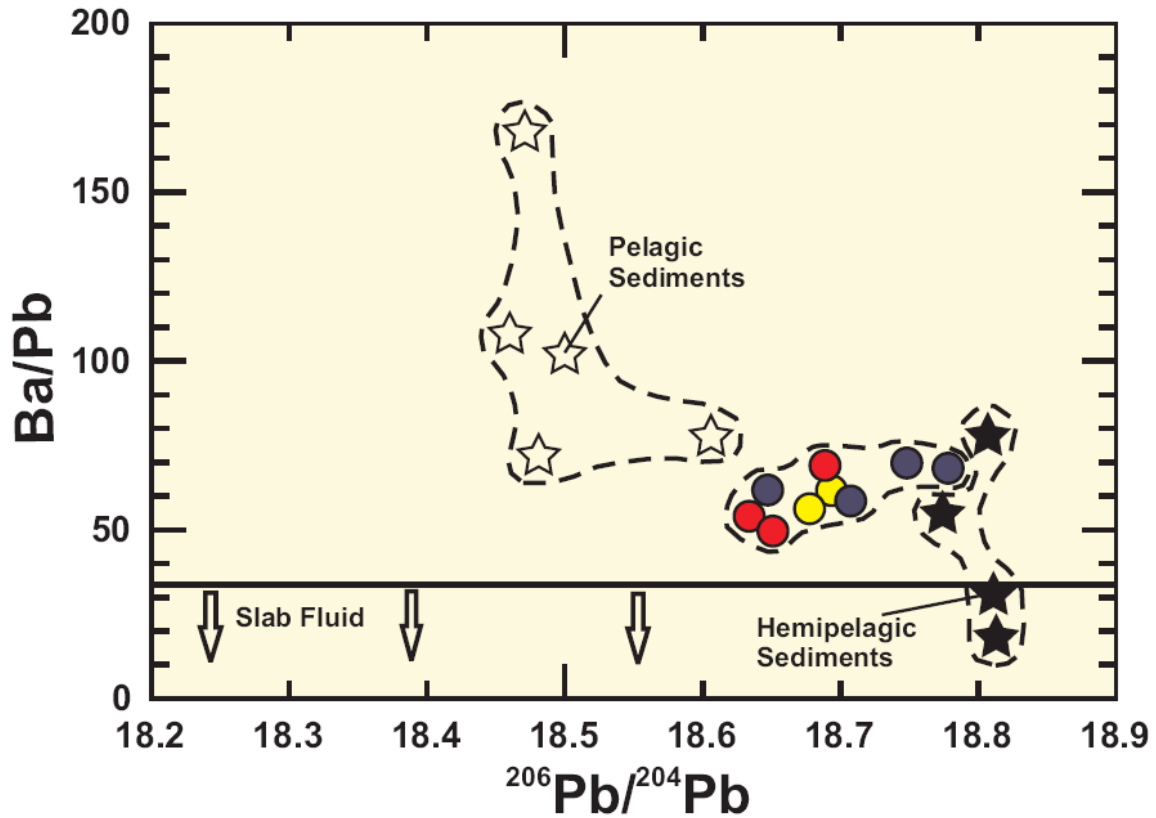


Figure 15. Ba/Pb versus  $^{206}\text{Pb}/^{204}\text{Pb}$  for SCVF lavas, Mexican sediment, N-MORB and AOC. The low-Nb group SCVF lavas have higher Ba/Pb ratios than N-MORB or AOC, requiring a sediment-derived fluid contribution to their mantle source (Sediment, AOC, and N-MORB data from LaGatta, 2003; Gomez-Tuena et al., 2007; and Sun and McDonough, 1989) Symbols as in figs. 11 and 13.

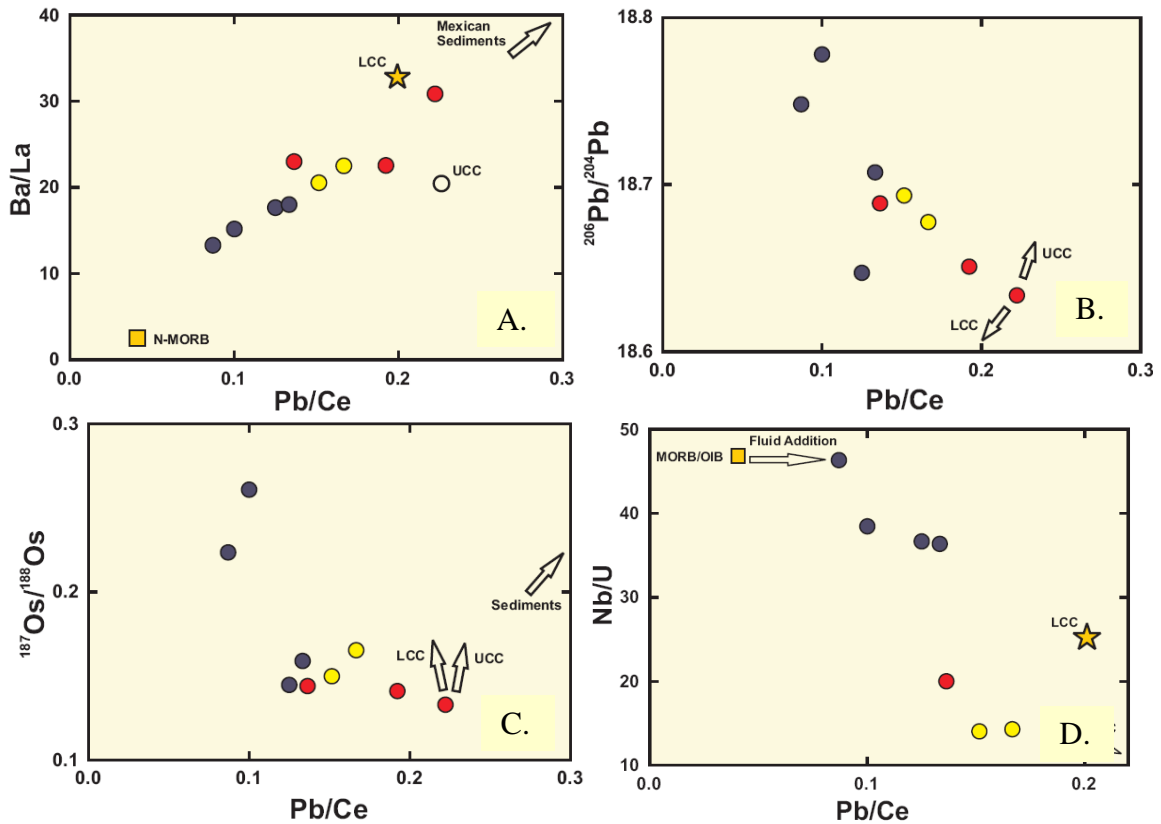


Figure 16. (a) Ba/La, (b)  $^{206}\text{Pb}/^{204}\text{Pb}$ , (c)  $^{187}\text{Os}/^{188}\text{Os}$  and (d) Nb/U versus Pb/Ce showing ranges in SCVF lavas. The high-Nb group samples are characterized by lower Pb/Ce and Ba/Nb ratios, suggestive of lesser fluid addition or a less depleted source compared to that of the low-Nb group source. The negative correlations of Pb/Ce with  $^{187}\text{Os}/^{188}\text{Os}$  and  $^{206}\text{Pb}/^{204}\text{Pb}$  are opposite that expected if the signatures of the high-Nb group resulted from crustal assimilation. (Crust, sediment, MORB, and OIB data from Rudnick and Gao, 2003; Hofmann et al., 1986; Gomez-Tuena et al., 2007; Zartman and Haines, 1988; LaGatta, 2003; Saal et al., 1998; Peucker-Ehrenbrink and Jahn, 2001; Sun and McDonough, 1989).

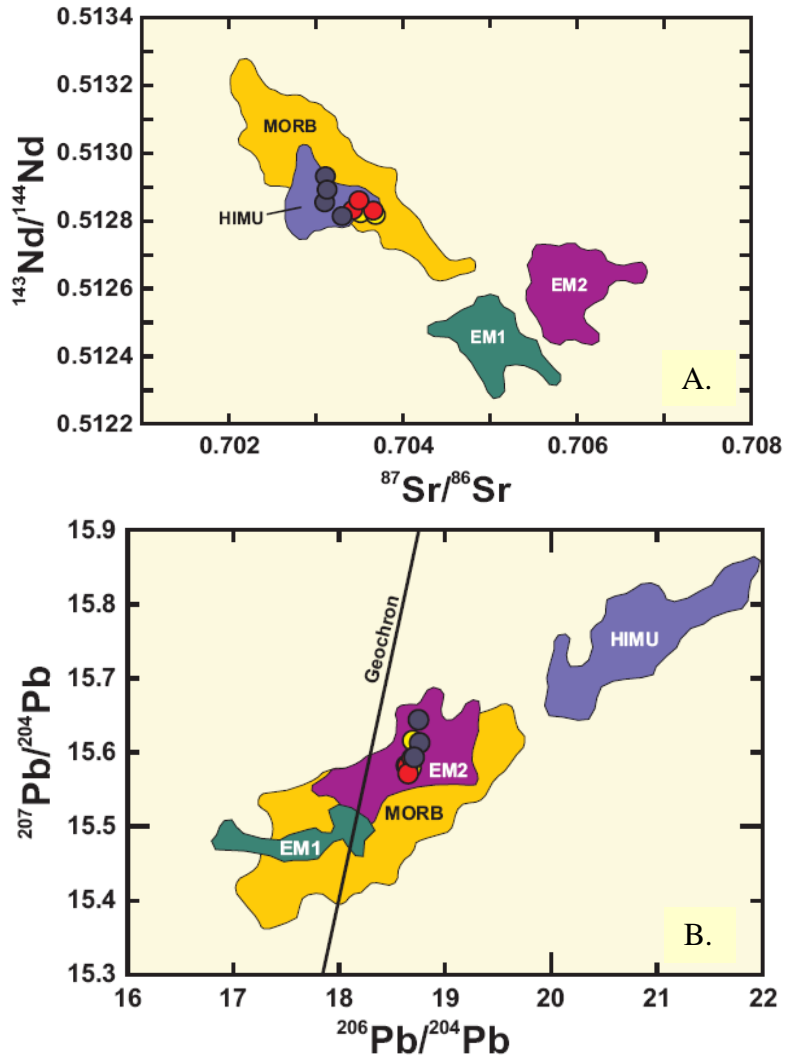


Figure 17. (after Hofmann, 1997). (a)  $^{143}\text{Nd}/^{144}\text{Nd}$  versus  $^{87}\text{Sr}/^{86}\text{Sr}$  and (b)  $^{206}\text{Pb}/^{204}\text{Pb}$  versus  $^{207}\text{Pb}/^{204}\text{Pb}$  showing isotopic compositions of SCVF lavas compared to MORB and HIMU, EM1 and EM2 type OIB. The SCVF lavas do not match the compositions of any OIB endmembers in all of the radiogenic isotope systems.

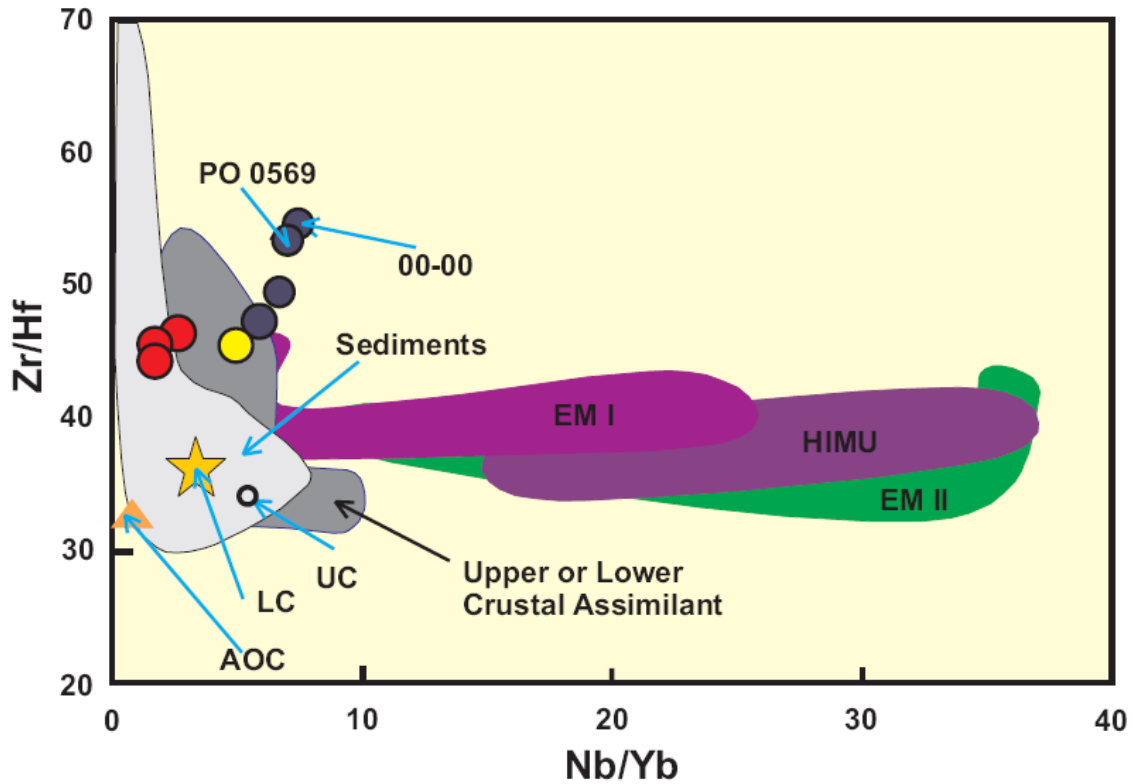


Figure 18. Zr/Hf vs Nb/Yb, showing the range for SCVF lavas compared to average upper and lower crust, AOC, OIB, and Mexican calculated bulk sediment, none of which exhibit Zr/Hf ratios as high as the high-Nb group SCVF lavas. (Literature data from Schaaf et al., 1994; LaGatta, 2003; Plank and Langmuir, 1998; Gomez-Tuena et al., 2007; Verma, 2000; Palacz and Saunders, 1986; Humphris and Thompson, 1983; Rudnick and Gao, 2003).

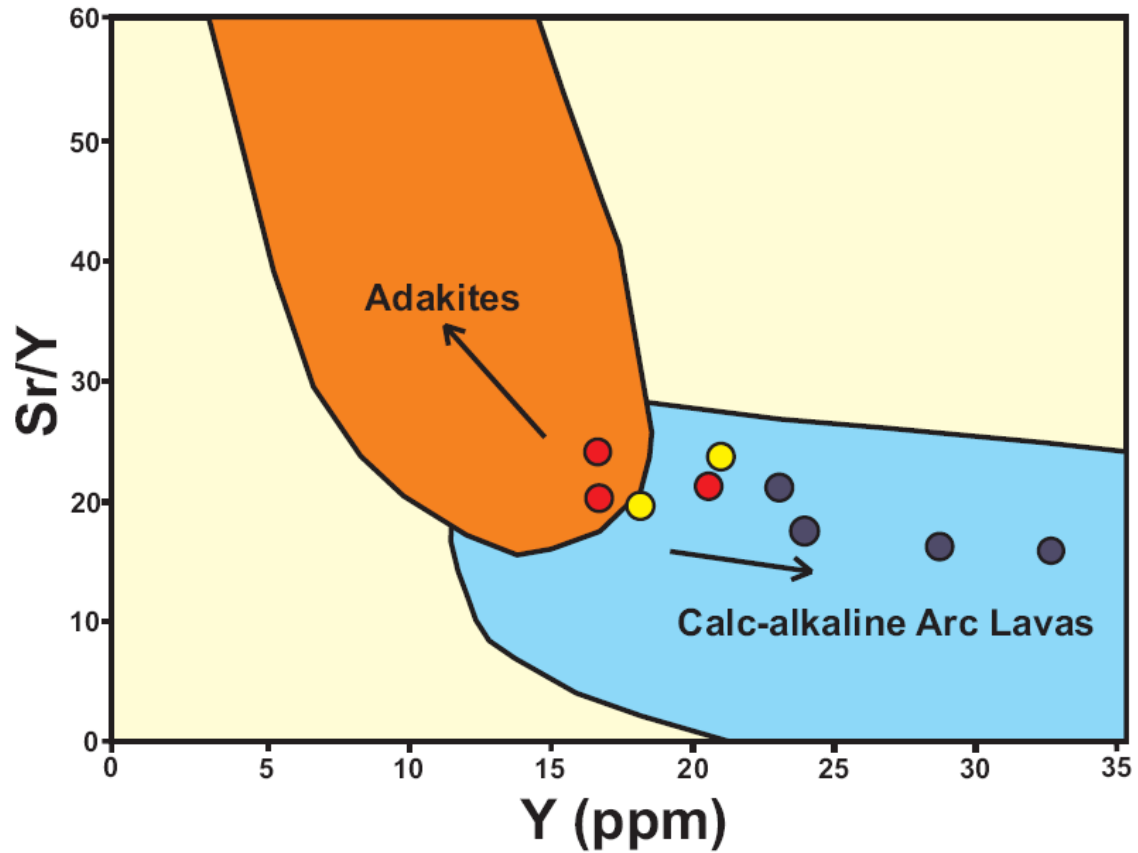


Figure 19. (after Defant and Drummond, 1990). Sr/Y vs Y, showing the compositional ranges for calc-alkaline arc magmas and adakitic magmas inferred to represent slab melts. Most of the samples from this study fall in the island arc field, and the high-Nb group samples from the SCVF trend towards lower Sr/Y and higher Y, inconsistent with a slab melt contribution to their source.

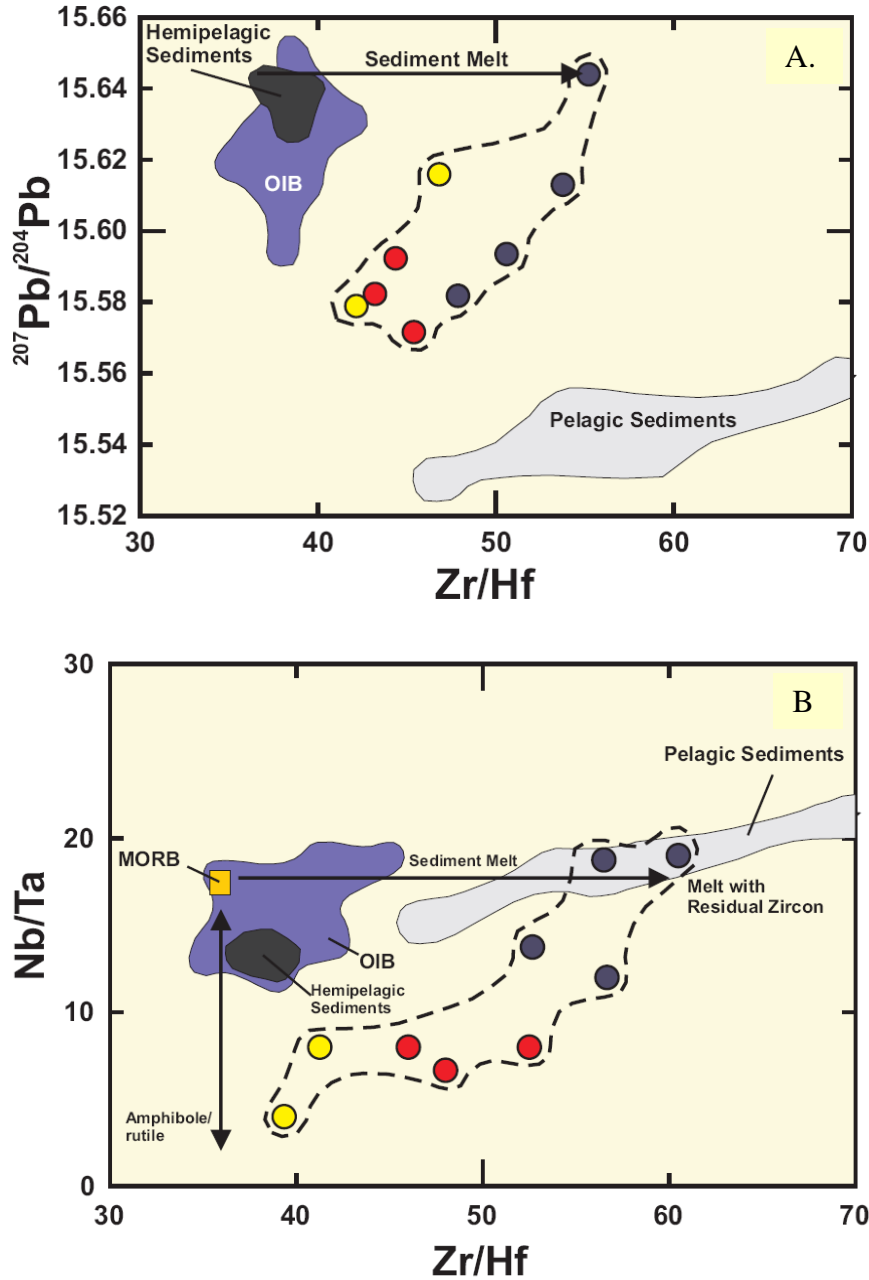


Figure 20. (a)  $^{207}\text{Pb}/^{204}\text{Pb}$  and (b) Nb/Ta versus Zr/Hf, showing the ranges in SCVF lavas compared to N-MORB OIB and Mexican sediments. The strongly suprachondritic Zr/Hf ratios of the high-Nb group SCVF lavas may be indicative of a sediment melt component in the mantle source, in which sediment melting in the presence of residual zircon with  $D_{\text{Zr}} < D_{\text{Hf}}$ . (Literature data for MORB, OIB, and Mexican sediment from LaGatta, 2003; Sun and McDonough, 1989; Humphris and Thompson, 1983; and Palacz and Saunders, 1986).

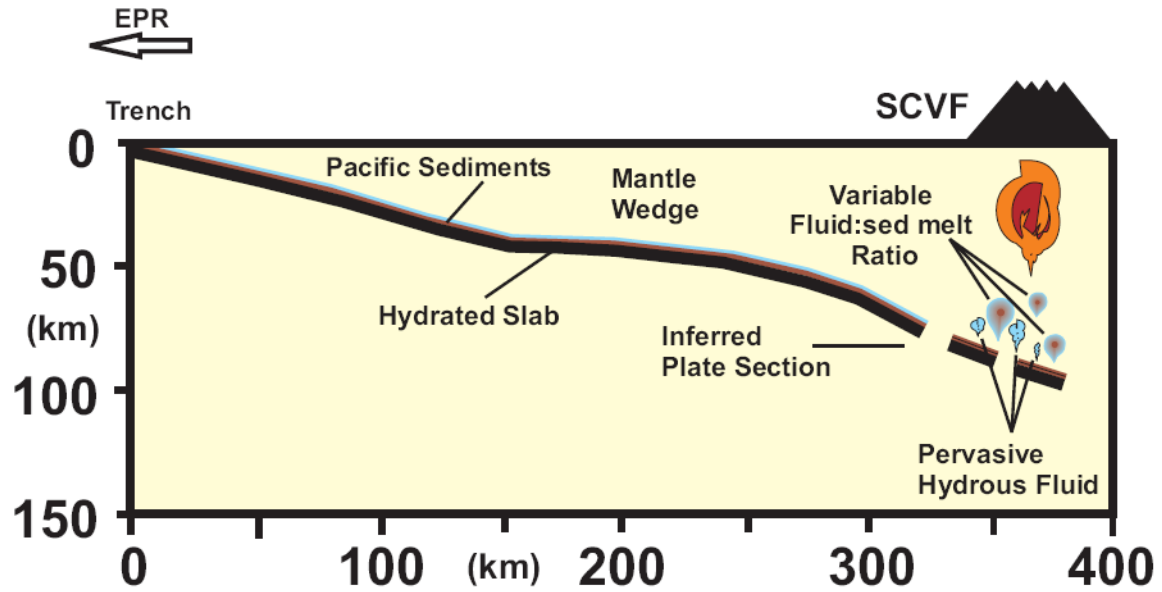


Figure 21. (after Pardo and Suarez, 1995; LaGatta, 2003). Cartoon diagram illustrating a model of the processes that may be occurring in the SCVF, including subduction and dehydration of the Cocos lithosphere and associated pelagic and hemipelagic sediment. Regions receiving a hydrous fluid flux yield the low-Nb group magmas. Regions of the mantle wedge that are also infiltrated by a hemipelagic sediment melt (thus a lower hydrous fluid:sediment melt ratio) produce magmas characteristic of the high-Nb group.

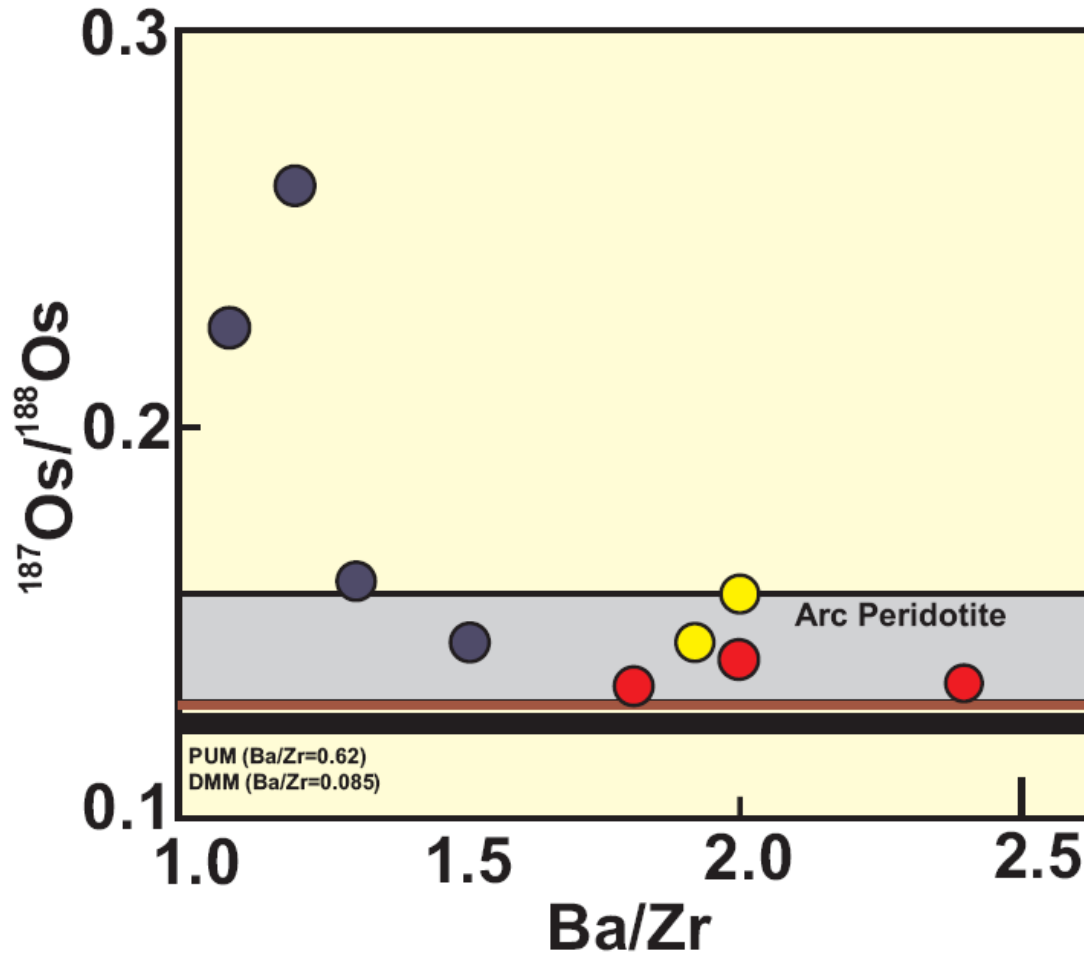


Figure 22.  $^{187}\text{Os}/^{188}\text{Os}$  versus Ba/Zr for SCVF lavas, arc peridotites, MORB mantle and PUM. The strongly hyperbolic, negative correlation of the SCVF lavas is indicative of two-component mixing in which both mixing endmembers are more radiogenic in Os than MORB mantle, and suggests that both hydrous fluid as well as sediment melt can contribute radiogenic Os to the mantle wedge during subduction. (Arc peridotite data from Brandon et al., 1996; Widom et al., 2003; Saha et al., 2005; DMM/N-MORB values from Snow and Reisberg, 1995; Sun and McDonough, 1989; Meisel et al., 2001).

## References

- Alves, S., Allegre, C., Capmas, F., Schiano, P., 2002. Osmium isotope binary mixing arrays in arc volcanism. *Earth and Planetary Science Letters*, 198: 355-369.
- Becker, H., 2000. Re-Os fractionation in eclogites and blueschists and the implications for recycling of oceanic crust into the mantle, *Earth and Planetary Science Letters*, 177: 287-300.
- Blatter, D. L., Farmer, G. L., Carmichael, I.S.E., 2007. A north-south transect across the central Mexican volcanic belt at approximately 100 degrees W; spatial distribution, petrological, geochemical, and isotopic characteristics of quaternary volcanism. *Journal of Petrology*, 48: 901-950.
- Bloomfield, K., 1975. A late quaternary monogenetic field in central Mexico. *Geologic Research*, 64: 476-497.
- Borg, L., Brandon, A., Clynne, M., Walker, R., 2000. Re-Os isotopic systematic of primitive lavas from the Lassen region of the Cascade arc, California. *Earth and Planetary Science Letters*, 177: 301-317.
- Brandon, A.D., Creaser, R.A., Shirey, S.B., Carlson, R.W., 1996. Osmium recycling in subduction zones. *Science*, 272: 861-864.
- Brenan, J., Shaw, H., Phinney, D., 1994. Rutile-aqueous fluid partitioning of Nb, Ta, Hf, Zr, U and Th: implications for high field strength element depletions in island-arc basalts. *Earth and Planetary Science Letters*, 128: 327-339.
- Brenan, J., Shaw, H., Ryerson, F., Phinney, D. 1995. Mineral-aqueous fluid partitioning of trace elements at 900C and 2.0 GPa: constraints on the trace element chemistry of mantle and deep crustal fluids. *Geochimica Cosmochimica Acta*, 59: 3331-3350.
- Chadwick, J.P., Troll, V.R., Ginibre, C., Morgan, D., Gertisser, R., Waight, T.E., Davidson, J.P., 2007. Carbonate assimilation at Merapi Volcano, Java, Indonesia: insights from crystal isotope stratigraphy. *Journal of Petrology*, 48, 9: 1793 – 1812.
- Chesley, J., Ferrari, L., Gomez-Tuena, A., Righter, K., Ruiz, J., 2002. Source contamination versus assimilation; an example from the Trans-Mexican volcanic arc. *Earth and Planetary Science Letters*, 195: 211-221.
- Chesley, J., Righter, K., Ruiz, J., 2004. Large-scale mantle metasomatism: a Re-Os perspective. *Earth and Planetary Science Letters*, 219: 49-60.

- Cohen, A.S., and Waters, F.G., 1996. Separation of osmium from geological materials by solvent extraction for analysis by thermal ionization mass spectrometry. *Analytica Chimica Acta* 332: 269–275.
- Couch, R. and Woodcock, S., 1981. Gravity and structure of the continental margins of southwestern Mexico and northwestern Guatemala. *Journal of Geophysical Research*, 86: 1829-1840.
- Defant, M.J. and Drummond, M.S., 1990. Derivation of some modern arc magmas by melting of young subducted lithosphere. *Letters to Nature*, 347: 662-65.
- Demets, C., Gordon, R., Argus, D., Stein, S., 1990. Current plate motions, *Geophysical Research*. 101: 425-478.
- Demets, C., and Stein, S., 1990. Present-day kinematics of the Rivera plate and implications for tectonics in southwestern Mexico. *Journal of Geophysical Research*, 95: 931-21, 948.
- DePaolo, D.J., 1981. Trace element and isotopic effects of combined wallrock assimilation and fractional crystallization. *Earth and Planetary Science Letters*. 53: 189 – 202.
- DuFrane, S.A., Turner, S.P., Dosseto, A., van Soest, M., 2009. Reappraisal of fluid and sediment contributions to Lesser Antilles magmas. *Chemical Geology* 265: 272-278.
- Eisele, J., Sharma, M., Galer, S.J.G., Blicher-Toft, J., Devey, C.W., Hofmann, A.W., 2002. The role of sediment recycling in EM I inferred from Os, Pb, Hf, Nd, Sr isotope and trace element systematic of the Pitcairn hotspot. *Earth and Planetary Science Letters*, 196: 197 – 212.
- Esperanca, S., Carlson, R.W., Shirey, S.B., Smith, D., 1997. Dating crust-mantle separation: Re-Os isotopic study of mafic xenoliths from central Arizona. *Geology*, 25: 651-654.
- Ferrari, L., Conticelli, S., Vaggelli, G., Petrone, C., Manetti, P., 2000. Late Miocene volcanism and intra-arc tectonics during the early development of the Trans-Mexican Volcanic Belt. *Tectonophysics*, 318: 161-185.
- Ferrari, L., Petrone, C., Francalanci, L., 2001. Generation of oceanic-island basalt-type volcanism in the western Trans-Mexican volcanic belt by slab rollback, asthenosphere infiltration, and variable flux melting. *Geology*, 29: 507-510.
- Foley, S.F., Tiepolo, M., Vannucci, R., 2002. Growth of early continental crust controlled by melting of amphibolite in subduction zones. *Nature*, 417: 837–840.

- Fries, C., 1962. Bosquejo geologico de las partes central y occidental del Estado de Morelos y areas contiguas de Guerero y Mexico. 20<sup>th</sup> International Geological Congress, 17-53.
- Gannoun, A., Burton, K.W., Thomas, L.E., Parkinson, I.J., van Calsteren, P., Schiano, P., 2004. Osmium Isotope Heterogeneity in the Constituent Phases of Mid-Ocean Ridge Basalts. *Science*, 303: 70-72.
- Gannoun, A., Burton, K.W., Parkinson, I.J., Alard, O., Schiano, P., Thomas, L.E., 2007. The scale and origin of the osmium isotope variations in mid-ocean ridge basalts. *Earth and Planetary Science Letters*, 259: 541 – 556.
- Gill, J.B., 1981. *Orogenic Andesites and Plate Tectonics*. Minerals and Rocks. Berlin, Heidelberg, New York: Springer-Verlag. 16: 390pp.
- Gomez-Tuena, A., Langmuir, C.H., Goldstein, S.L., Straub, S.M., Ortega-Gutierrez, F., 2007. Geochemical Evidence for Slab Melting in the Trans-Mexican Volcanic Belt. *Journal of Petrology*, 48: 537-562.
- Gunn, B., and Mooser, F., 1971. Geochemistry of the volcanics of central Mexico. *Bulletin of Volcanology*, 34: 577-616.
- Hart, S.R., Blusztajn, J., Dick, H.J.B., Meyer, P.S. and Muehlenbachs, K. 1999. The fingerprint of seawater circulation in a 500-meter section of ocean crust gabbros. *Geochimica et Cosmochimica Acta*, 63: 4,059-4,080.
- Hauri, E.H., and Hart, S.R., 1993. Re-Os isotope systematic of HIMU and EM II oceanic island basalts from the south Pacific Ocean. *Earth and Planetary Science Letters*, 114: 353 – 371.
- Hofmann, A.W., Jochum, K.P., Seufert, M., White, W.M., 1986. Nb and Pb in oceanic basalts: new constraints on mantle evolution. *Earth and Planetary Science Letters*, 79: 33–45.
- Hofmann, A.W., 1997. Mantle geochemistry: the message from oceanic volcanism. *Nature*, 385: 219-229.
- Humphris, S.E. and Thompson, G., 1983. Geochemistry of rare earth elements in basalts from the Walvis Ridge: implications for its origin and evolution. *Earth and Planetary Science Letters*, 66: 223-242.
- Ito, E., White, W.M., Gopel, C., 1987. The O, Sr, Nd, Pb isotope geochemistry of MORB. *Chemical Geology*, 62: 157 – 176.

- Johnson, M.C., and Plank, T., 1999. Dehydration and melting experiments constrain the fate of subducted sediments. *Geochemistry, Geophysics, Geosystems—G 3*, 1(1), 1999GC000014.
- Katoh, S., Danhara, T., Hart, W.K., Gabriel, G.W., 1999. Use of sodium polytungstate solution in the purification of volcanic glass shards for bulk chemical analysis. *Nature of Human Activity*, 4: 45– 54.
- Kay, R.W., 1978. Aleutian magnesian andesites: melts from subducted Pacific ocean crust. *Journal of Volcanology and Geothermal Research*, 4: 497-522.
- Kelemen, P.B., Hanghoj, K., Greene, A.R., 2004. One View of the Geochemistry of Subduction-related Magmatic Arcs, with an Emphasis on Primitive Andesite and Lower Crust. *Treatise on Geochemistry*. Holland, H.D. and Turekian, K.K. (Editors), Elsevier, Amsterdam, 3: 593-659.
- Kelley, K.A., Plank, T., Ludden, J., Staudegel, H., 2003. Composition of altered oceanic crust at ODP Sites 801 and 1149. *Geochemistry, Geophysics, Geosystems—G 3*, 4(6). 2002GC000435.
- Klein, E.M. 2004. *Geochemistry of the Igneous Oceanic Crust*. In: *Treatise on Geochemistry*. Holland, H.D. and Turekian, K.K. (Editors), Elsevier, Amsterdam. 3: 433-463.
- Kogiso T., Tatsumi Y., Nakano S., 1997. Trace element transport during dehydration processes in the subducted oceanic crust: 1. Experiments and implications for the origin of ocean island basalts. *Earth and Planetary Science Letters*, 148: 193–206.
- LaGatta, A.B, 2003. *Arc Magma Genesis in the Eastern Mexican Volcanic Belt*. Thesis, Columbia University.
- Le Bas, M.J., Le Maitre, R.W., Streckeisen, A., Zanettin, B., 1986. A chemical classification of volcanic rocks based on the total alkali-silica diagram, *Journal of Petrology*, 27: 745–750.
- Lehnert, K., Su, Y., Langmuir, C.H., Sarbas, B. and Nohl, U., 2000. A global geochemical database structure for rocks. *Geochemistry, Geophysics, Geosystems—G 3*, 1(5). 1999GC000026.
- Lassiter, J.C., and Luhr, J.F., 2001. Osmium abundance and isotope variations in mafic Mexican volcanic rocks; evidence for crustal contamination and constraints on the geochemical behavior of osmium during partial melting and fractional crystallization. *Geochemistry, Geophysics, Geosystems – G 3*, 2 200GC000116.

- Linnen, R.L., Keppler, H., 2002. Melt composition control of Zr/Hf fractionation in magmatic processes. *Geochimica et Cosmochimica Acta*, 66: 3293-3301.
- Marquez, A., Verma, S., Anguita, F., Oyarzun, R., Brandle, J., 1999. Tectonics and volcanism of Sierra Chichinautzin: extension at the front of the Central Trans-Mexican Volcanic Belt. *Journal of Volcanology and Geothermal Research*, 91: 125-150.
- McLennan, S., Taylor, S., McCulloch, M., Maynard, J., 1990. Geochemical and Nd-Sr isotopic composition of deep-sea turbidites: crustal evolution and plate tectonic associations. *Geochimica et Cosmochimica Acta*, 54: 2015-2050.
- Martin, A., 1982. Monogenetic volcanism in Sierra Chichinautzin, Mexico. *Bulletin of Volcanology*, 45: 9-24.
- Mearon, S., Paytan, A., Bralower, T. J., 2003. Cretaceous strontium isotope stratigraphy using marine barite. *Geology (Boulder)*, 31: 15-18.
- Meisel, T., Walker, R.J., Irving, A.J., Lorand, J.P., 2001. Osmium isotopic compositions of mantle xenoliths: A global perspective. *Geochimica et Cosmochimica Acta* 65: 1311– 1323.
- Mooser, F., 1962. Bosquejo geológico del extreme sur de la Cuenca de Mexico, 20<sup>th</sup> annual Geological Congress, 9-16.
- Mooser, F., Nairn, A., Negendank, J., 1974. Paleomagnetic investigations of the Tertiary and Quaternary igneous rocks. *Geologic Research*, 63: 451-483.
- Morris, J.D., Leeman, W.P. Tera, F. 1990. The subducted component in island arc lavas: constraints from Be isotopes and B–Be systematics. *Nature*, 344: 31–36.
- Nier, A.O., 1950. A redetermination of the relative abundances of the isotopes of carbon, nitrogen, oxygen, argon and potassium. *Physics Reviews*, 77: 789–793.
- Niu, Y., Regelous, M., Wendt, I., Batiza, R., O'Hara, M., 2002. Geochemistry of near-EPR seamounts: importance of source vs. process and the origin of enriched mantle component. *Earth and Planetary Science Letters*, 199: 327-345.
- Ortega-Gutierrez, F., Elias-Herrera, M., Davalos-Elizondo, M.G., 2008. On the nature and role of the lower crust in the volcanic front of the Trans-Mexican Volcanic Belt and its fore-arc region, southern and central Mexico. *Revista Mexicana de Ciencias Geológicas*, 25: 346-364.
- Palacz, Z.A. and Saunders, A.D., 1986. Coupled trace element and isotope enrichment in the Cook-Austral-Samoa islands, southwest Pacific. *Earth and Planetary Science Letters*, 79: 270-280.

- Pardo, M., and Suarez, G., 1995. Shape of the subducted Rivera and Cocos plates in southern Mexico: Seismic and tectonic implications. *Journal of Geophysical Research*, 100: 12,357-12,373.
- Patino, L.C., Carr, M.J., Feigenson, M.D., 2000. Local and regional variations in Central American arc lavas controlled by variations in subducted sediment input. *Contributions to Mineralogy and Petrology*, 138: 265–283.
- Pearce, J.A., Baker, P.E., Harvey, P.K., Luff, I.W., 1995. Geochemical evidence for subduction fluxes, mantle melting and fractional crystallization beneath the south Sandwich Island arc. *Journal of Petrology*, 36: 1073 – 1109.
- Pearce, J.A., Stern, R.J., Bloomer, S.H., Fryer, P., 2005. Geochemical mapping of the Mariana arc-basin system: implications for the nature and distribution of subduction components. *Geochemistry, Geophysics, Geosystems—G3*, 7 2004GC000895.
- Peate, D.W., and Pearce, J.A., 1998. Causes of spatial compositional variations in Mariana arc lavas: Trace element evidence. *The Island Arc*, 7: 479-495.
- Petrone, C., Francalanci, L., Carlson, R., Ferrari, L., Conticelli, S., 2003. Unusual coexistence of subduction-related and intraplate-type magmatism: Sr, Nd, and Pb isotope and trace element data from the magmatism of the San Pedro-Ceboruco graben (Nayarit, Mexico). *Chemical Geology*, 193: 1-24.
- Peucker-Ehrenbrink, B., Ravizza, G., Hofmann, A.W., 1995. The marine  $^{187}\text{Os}/^{186}\text{Os}$  record of the past 80 million years. *Earth and Planetary Science Letters*, 130: 155–167.
- Peucker-Ehrenbrink, B., and Jahn, B., 2001. Rhenium-Osmium isotope systematics and platinum group element concentrations: Loess and the upper continental crust, *Geochemistry, Geophysics, Geosystems – G 3*, 2 GC000172 (2001).
- Pin, C., and Zalduegui, J.F.S., 1997. Sequential separation of light rare earth elements, thorium and uranium by miniaturized extraction chromatography: application to isotopic analyses of silicate rocks. *Analytica Chimica Acta*, 339: 79–89.
- Plank, T., and Langmuir, C.H., 1998. The chemical composition of subducting sediment and its consequences for the crust and mantle. *Chemical Geology*, 145: 325-394.
- Rehkamper, M. and Hofmann, A.W. 1997. Recycled ocean crust and sediment in Indian Ocean MORB. *Earth and Planetary Science Letters*, 147(1-4): 93-106.
- Reisberg, L., Zindler, A., Marcantonio, F., White, W., Wyman, D., Weaver, B., 1993. Os isotope systematic in ocean island basalts. *Earth and Planetary Science Letters*, 120: 149 – 167.

- Roy-Barman, M., 1993. Mesure du rapport  $^{187}\text{Os}/^{186}\text{Os}$  dans les basalts et peridotites: contribution a la systematique  $^{187}\text{Re}/^{186}\text{Os}$  dans le manteau, Thesis, Univ. Paris 7.
- Roy-Barman, M., and Allegre, C.J., 1995.  $^{187}\text{Os}/^{186}\text{Os}$  in ocean island basalts: tracing oceanic crust recycling in the mantle. *Earth and Planetary Science Letters*, 129: 145–161.
- Rudnick, R. and Gao, S., 2003. *Treatise on Geochemistry: Composition of the Continental Crust*, Elsevier Ltd., Chapter 3, 1-64.
- Saal, A., Rudnick, R., Ravizza, G., Hart, S., 1998. Re-Os isotope evidence for the composition, formation and age of the lower continental crust. *Nature*, 393: 58-61.
- Saha, A., Basu, A.R., Jacobsen, S.B., Poreda, R.J., Yin, Q.Z., Yogodzinski, G.M., 2005. Slab devolatilization and Os and Pb mobility in the mantle wedge of the Kamchatka arc. *Earth and Planetary Science Letters*, 236: 182-194.
- Salters, V. J. M., and Stracke, A., 2004. Composition of the depleted mantle. *Geochemistry Geophysics Geosystems*, 5, Q05004, doi:10.1029/2003GC000597.
- Schaaf, P., Heinrich, W., Besch, T., 1994. Composition and Sm-Nd isotopic data of the lower crust beneath San Luis Potosi, central Mexico: Evidence from a granulite-facies xenolith suite. *Chemical Geology*, 118: 63-84.
- Schaaf, P., Stimac, J., Siebe, C., Macias, J., 2005. Geochemical evidence for mantle origin and crustal processes in volcanic rocks from Popocatepetl and surrounding monogenetic volcanoes, Central Mexico. *Journal of Petrology*, 46: 1243-1282.
- Schmidt, M.W., Dardon, A., Chazot, G., Vannucci, R. 2004. Rutile-melt partitioning of Nb and Ta dependent on melt composition and Nb/Ta fractionation in the Earth. *Earth and Planetary Science Letters*, 226: 415-432.
- Shirey, S., and Walker, R., 1998. The Re-Os isotope system in chosmochemistry and high-temperature geochemistry. *Annual Reviews of Earth and Planetary Science Letters*, 26: 423-500.
- Siebe, C., Rodriguez-Lara, V., Schaaf, P., Abrams, M., 2004. Geochemistry, Sr-Nd isotope composition, and tectonic setting of Holocene Pelado, Guespalapa and Chichinautzin scoria cones, south of Mexico City. *Journal of Volcanology and Geothermal Research*, 130: 197-226.

- Siebe, C., and Macias, J.L., 2006. Volcanic hazards in the Mexico City metropolitan area from eruptions at Popocatepetl, Nevado de Toluca, and Jocotitlan stratovolcanoes and monogenetic scoria cones in the Sierra Chichinautzin Volcanic Field. Geological Society of America, Special Paper #402: 253 – 329.
- Snow, J. and Reisberg, L., 1995. Os isotopic systematics of the MORB mantle: results from altered abyssal peridotites. Earth and Planetary Science Letters, 133: 411-21.
- Snyder, D.C., 2005. Processes and Time Scales of Differentiation in Silicic Magma Chambers: Chemical and Isotopic Investigations. PhD dissertation, Miami University, 227p.
- Sun, S.-s., McDonough, W.F., 1989. Chemical and isotopic systematic of oceanic basalts: implications for mantle composition and processes. Geological Society Special Publication 42: 313-345.
- Suzuki, K., Aizawa, Y., Tatsumi, Y., 2003. Osmium transport during dehydration processes in the subducted slab: Experiments and implications for the Os isotopic compositions of arc magmas. Frontier Research on Earth Evolution, IFree Report for 2001–2002, 1: 107–110.
- Suzuki, K., and Tatsumi, Y., 2006. Re-Os systematic of high-Mg andesites and basalts from the Setouchi volcanic belt, SW Japan. Geochemical Journal, 40: 297-307.
- Swinamer, R., 1989. The Geomorphology, Geochemistry, and petrogenesis of the volcanic rocks in the Sierra del Chichinautzin, Mexico, M. Thesis, Queen's University, Kingston, ON, 212p.
- Tatsumi, Y., 2005. The subduction factory: How it operates in the evolving Earth. GSA Today, 15: 4 – 10.
- Tatsumi, Y., and Kogiso, T., 1997, Trace element transport during dehydration processes in the subducted oceanic crust: 2. Origin of chemical and physical characteristics in arc magmatism. Earth and Planetary Science Letters, 148: 207-221.
- Tiepolo, M., Vannucci, R., Oberti, R., Foley, S., Bottazzi, P., Zanetti, A., 2000. Nb and Ta incorporation and fractionation in titanian pargasite and kaersutite: crystal-chemical constraints and implications for natural systems. Earth and Planetary Science Letters, 176: 185-201.
- Todt, W., Cliff, R.A., Hanser, A., Hofmann, A.W., 1996. Evaluation of a  $^{202}\text{Pb}$ – $^{205}\text{Pb}$  double spike for high precision lead isotope analysis. In: Basu, A., Hart, S. (Eds.), Earth Processes: Reading the Isotopic Code. AGU Mongraph. 95: 429–437.
- Tollstrup, D.L., and Gill, J.B., 2005. Hafnium systematics of the Mariana Arc; evidence for sediment melt and residual phases. Geology (Boulder), 33: 737-740.

- Valdez-Moreno, G., Schaaf, P., Macias, J.L., Kusakabe, M., 2006. New Sr-Nd-Pb-O isotope data for Colima volcano and evidence for the nature of the local basement. *Geological Society of America*, 45-63.
- Verma, S. P., 1999. Geochemistry of evolved magmas and their relationship to subduction-unrelated mafic volcanism at the volcanic front of the central Mexican Volcanic Belt. *Journal of Volcanology and Geothermal Research*, 93: 151–171.
- Verma, S.P., 2000. Geochemistry of the subducting Cocos plate and the origin of subduction-unrelated mafic volcanism at the volcanic front of the central Mexican Volcanic Belt. *Geological Society of America. Special Paper 334*, 195-222.
- Walker, R.J., Carlson, R.W., Shirey, S.B., Boyd, S.B., 1989. Os, Sr,Nd and Pb isotope systematics of southern African peridotite xenoliths: implications for the chemical evolution of subcontinental mantle. *Geochimica et Cosmochimica Acta*, 53: 1583–1595.
- Walker, J.A., Patino, L.C., Cameron, B.I., Carr, M.J., 2000. Petrogenetic insights provided by compositional transects across the Central American Arc. *Journal of Geophysical Research*, 105: 18,949-18,963.
- Wallace, and P.J., Carmichael, I.S.E., 1999. Quaternary volcanism near the Valley of Mexico: implications for subduction zone magmatism and the effects of crustal thickness variations on primitive magma compositions. *Contributions to Mineral Petrology*, 135: 291-314.
- Weaver, B., 1991. Trace element evidence for the origin of ocean-island basalts. *Geology*, 19: 123 – 126.
- Widom E. and Shirey S.B., 1996. Os isotope systematics in the Azores: implications for mantle plume sources. *Earth and Planetary Science Letters*, 142: 451-465.
- Widom, E., Kepezhinskias, P., Defant, M., 2003. The nature of metasomatism in the sub-arc mantle wedge: evidence from Re-Os isotopes in Kamchatka peridotite xenoliths. *Chemical Geology*, 196: 283–306.
- Xiong, Y., Wood, S.A., 2000. Experimental quantification of hydrothermal solubility of platinum-group elements with special reference to porphyry copper environments. *Mineral Petrology*, 68: 1 – 28.
- Zartman, R.E., and Haines, S.M., 1988. The plumbotectonic model for Pb isotopic systematic among major terrestrial reservoirs—a case for bi-directional transport. *Geochimica et Cosmochimica Acta*. 52: 1327 – 1359.